Mesoporous bio-materials synthesized with corn and potato starches applied in CO_2 capture

S.G. Aspromonte, M.A. Tavella, M. Albarracín, A.V. Boix

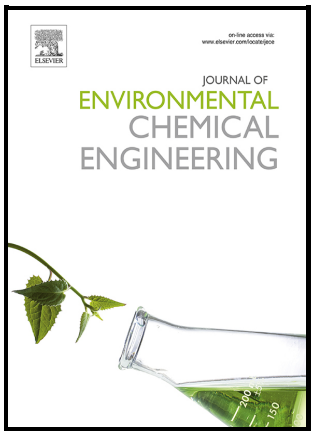

PII: S2213-3437(23)00281-6

DOI: https://doi.org/10.1016/j.jece.2023.109542

Reference: JECE109542

To appear in: *Journal of Environmental Chemical Engineering*

Received date: 16 November 2022
Revised date: 3 February 2023
Accepted date: 17 February 2023

Please cite this article as: S.G. Aspromonte, M.A. Tavella, M. Albarracín and A.V. Boix, Mesoporous bio-materials synthesized with corn and potato starches applied in CO_2 capture, *Journal of Environmental Chemical Engineering,* (2022) doi:https://doi.org/10.1016/j.jece.2023.109542

Mesoporous bio-materials synthesized with corn and potato starches applied in CO_2 capture

S.G. Aspromonte[1,*], M.A. Tavella[1], M. Albarracín[2], A.V. Boix[1]

[1] Research Institute in Catalysis and Petrochemistry – INCAPE (FIQ UNL-CONICET), Santiago del Estero 2829, 3000, Santa Fe, Argentina

[2] Institute of Food Technology - ITA (FIQ-UNL) – 1º de mayo 3150, 3000, Santa Fe, Argentina.

Corresponding author. Tel: +54 342 4536861

[*]E-mail address: saspromonte@fiq.unl.edu.ar

ABSTRACT

The development of environmentally friendly techniques to obtain mesoporous solids allows the construction of new and better materials, making potential use of natural resources. In this study, mesoporous silica with high specific surface area and controlled porosity is synthesized by a novel and facile method, which employs potato or corn starches as directing structure agent. Using SEM microscopy, the ellipsoidal morphology of potato starch and the irregular and polygonal shape of corn starch were determined. Pattern A and B were identified by XRD, corresponding to samples of cereals and tubers, respectively. The stages of gelatinization and retrogradation of the starches were studied, obtaining mesoporous silicas with type IV adsorption/desorption isotherms and specific surface areas of 708.6 m^2g^{-1} with potato starch and 1018.1 m^2g^{-1} with corn starch for short gelatinization times (4 h, 353 K) and long retrogradation (14 h, 298 K). In addition, the use of HCl solution promoted the hydrolysis of starch in its monomeric unit (glucose) and the consequent bimolecular nucleophilic substitution with silica. The materials obtained presented a random mesoporous order and a CO_2 adsorption capacity at 373 K in the range between 150.2 and 131.4 mg CO_2 g^{-1}.

Keywords: Adsorption, Biomass, Bio-template, Carbon Dioxide, Preparation, Silica

1. INTRODUCTION

There is a growing commitment to the possibility of directing research and innovation efforts towards achieving eco-friendly technologies [1-3]. For this, a balance must be struck between economic, ecological, social and political sectors. In this context, the generation of materials from simpler and more economical compounds, under mild synthesis conditions, minimizing the use of energy and recycling already used materials or waste, is certainly of great scientific and economic interest [4-7].

Porous materials of different nature are widely studied, including crystalline aluminosilicates such as zeolites or mesoporous silicas such as MCM41, MCM48, SBA15, among others [8, 9]. These materials have aroused great interest because they overcome the limitations regarding pore size, facilitating the diffusion of voluminous reactive and products molecules to and from the active centers [10-12]. Several mechanisms of mesoporous synthesis are reported in the open literature [13, 14]. Among them, the use of structure directing agents (SDA) as patterns or templates, represents one of the conventional methods, simple and easy to reproduce [15]. This synthesis strategy is based on the interaction of inorganic precursors with organic molecules that direct the formation of pores around them. Many attempts have been made to synthesize mesoporous silica materials using anionic, cationic, non-ionic surfactants or a combination of them as surfactants [16, 17]. In particular, among the most commercially used are: (i) cationic surfactants, such as, n-hexadecyltrimethyl ammonium bromide (CTAB) employed in the MCM-41 synthesis [18, 19] and (ii) three-block copolymers (hydrophilic-hydrophobic-hydrophilic) as Pluronic for the SBA-15 production [20-22].

Although these structuring agents allow materials with hierarchical and stable porosity to be obtained, commercial templates are expensive and their complete removal temperature (~ 823 – 873 K) is high [23-25]. Hence, the need to select non-toxic, eco-friendly and inexpensive materials as SDA to synthesize porous materials.

In this sense, it is also possible to use structuring agents of biological or natural source in the preparation of mesoporous silica. Bio-template method is attractive in the preparation of porous materials. In this vein, compounds such as sponge [26], aminoacids [27] and cells [28] have

been used as templates to prepare porous silicon. In particular, natural wood [29] and phosphatidylcholine [30] were used to prepare porous titania. Zhang et al. [31] used poplar catkins as a bio-template to synthesize SnO_2 fibers. In addition, Ma and co-workers [32] reported the preparation of macro/meso-porous alumina with yeast cell as bio-template.

Recently, starch from different botanical nature and as an environmentally friendly, cheap and readily available natural resource has been used as a template to synthesize porous materials such as silicate monoliths [33], aluminosilicates [34], ZSM5 [35, 36], AlPO-n [37], TS-1 [38], Al_2O_3 [39], stoichiometric $LaAlO_3$ mixed oxides [40] and mordenite [41].

On the other hand, it is important to consider that mesoporous materials are used in a wide range of applications to reduce greenhouse gas (GHG) emissions. Among them, the generation of CO_2 has been subject of multiple studies in recent times [42]. The Carbon Dioxide Information Analysis Center (Division of Environmental Sciences of the OAK Ridge National Laboratory) of Tennessee (USA), established that from 1960 to the present time, the world average atmospheric concentration reached 400 parts by million [43]. It is estimated that, if GHG emissions continue at the current rate, the temperature of the earth surface could exceed historical values, with potentially harmful effects on the environment, biodiversity, and human incomes. Therefore, the development of effective methods to reduce the concentration of carbon dioxide in the atmosphere is essential. A viable route is the CO_2 capture through adsorption processes, which represents an attractive method due to its low energy requirement [44].

Different types of materials have been studied in the capture and conversion of CO_2 such as porous solid based on metal-organic frameworks (MOFs), zeolites, mesoporous silica, clay, carbons, porous organic polymers (POPs), hydrotalcite, organic-inorganic hybrids and metal oxides [45, 46].

The group of Calleja has extensive experience in the study of CO_2 capture using expanded pores MCM41 mesoporous materials [47], SBA-15 functionalized with amino groups [48] and HMS (high mesoporous silica) [49]. HMS adsorbent reported a CO_2 adsorption capacity of 4.19 mmol $CO_2 \cdot g^{-1}$ (363 K, 1 bar), while double-functionated MCM41 captured 1.75 $CO_2 \cdot g^{-1}$ at 318 K and 1 bar. Similarly, SBA-15 silica modified with PEI (polyethyleneimine) and TEPA

(tetraethylpolyamine) adsorbed 2.05 mmol $CO_2 \cdot g^{-1}$ (348 K, 1 bar) and 3.7 mmol $CO_2 \cdot g^{-1}$ (318 K, 1 bar), respectively.

Therefore, the aim of this work is to present a convenient approach to synthesize mesoporous silica using starch as a harmless and cheap resource. For this, the cooperative mechanism of hydrothermal synthesis is applied with potato and corn starches as structure directing agents. The starches were characterized by thermogravimetric analysis (TGA), X-ray diffraction (XRD), scanning electron microscopy (SEM) and Fourier transform infrared spectroscopy (FTIR). Through optical microscopy, the modification of the granule in aqueous suspension was analyzed at different temperatures (303 – 353 K), pH (acid, neutral and basic) and the influence of ethanol. Then, different times, temperatures and media were studied in the synthesis of mesoporous silica considering the stages of starches gelatinization and retrogradation. The synthesized solids were characterized with N_2 adsorption/desorption at 77 K and transmission electron microscopy (TEM). Analyzing the results obtained, a mechanism of the most promising synthesis route is proposed. Finally, the samples were evaluated for CO_2 adsorption at 373 K and compared with the results obtained by our group and the available literature.

2. MATERIAL AND METHODS

In order to obtain mesoporous silica through hydrothermal synthesis and using starch as a structuring agent, various factors that influenced the preparation steps were analyzed. First, corn and potato starches were characterized by X-Ray diffraction (XRD), Fourier Infrared spectroscopy (FTIR), thermogravimetric analysis (TGA), and scanning electron microscopy (SEM). Then, modification of the granule in aqueous suspension was studied at different temperatures, pH and the ethanol addition.

The properties of the solids obtained were characterized by N_2 adsorption/desorption at 77 K and transmission electron microscopy (TEM). Finally, the materials obtained were used as adsorbents for CO_2 capture at 373 K.

2.1 Physicochemical characterization of potato and corn starches

2.1.1 Morphology

The morphology of the starches was observed through scanning electron microscopy (SEM). For this, a bank SEM microscope, Phenom World model ProX (Holland), operated between 10 and 15 keV was used.

2.1.2 X-Ray diffraction (XRD)

The X-ray diffraction measurements were taken using a Shimadzu diffractometer XD-D1 model (Japan) operated with CuKα radiation at 30 kV and 40 mA, using a scanning rate of $1°\cdot min^{-1}$. The database employed was the one provided by the manufacturer.

2.1.3 Amylose content

For the determination of amylose content, the method of Belhadi et al. [50] was used. For this, 100 mg of sample were weighed, a treatment was carried out in a boiling water bath with NaOH and ethyl alcohol for 10 min. The pH of the sample was adjusted by adding acetic acid until reaching a pH between 8.6 and 9.8. An I_2/IK solution was added and finally, the absorbance of the blue complex formed was measured in a spectrophotometer at 620 nm (Spectronic Genesys

5 UV-Vis, Milton Roy, USA). Likewise, a calibration curve was obtained with an amylose standard (Sigma, USA) from which the total amylose content (wt. %) was calculated according to Equation 1:

$$\%\ Amylose = \frac{(A_{sample} - A_{blank}) - b}{m}\ x\ D\ x\ \frac{100}{p}\ x\ 100 \qquad \text{Eq. (1)}$$

Where, A_{sample} is the sample absorbance, A_{blank} is the absorbance of blank, b is the ordinate of the origin, m is the slope of the curve (mg ml^{-1}), D is the factor of dilution (ml ml^{-1}) and p is the sample weight (mg).

2.1.4 Fourier transform infrared spectroscopy (FTIR)

Fourier transform infrared spectroscopy (FTIR) was collected on a Shimadzu IR Prestige-21, model 8101M spectrometer (Japan) using mixtures of potato or corn starches with KBr, with a ratio of about 1 mg per 200 mg of KBr.

2.1.5 Thermogravimetric analysis (TGA)

Thermogravimetric analysis was conducted with a Mettler-Toledo TGA/SDTA851E instrument (USA). The operation was performed from 303 to 1173 K at a heating rate of 10 $K \cdot min^{-1}$ under nitrogen.

2.2 Study and characterization of aqueous starch suspensions

In order to reproduce the behavior of starch and approximate the studies to the synthesis process, the influence of temperature, pH and addition of ethanol in aqueous suspension of potato and corn starch suspensions was analyzed. The selected temperatures were 303, 323 and 353 K and acidic, neutral, or basic medium were studied by adding HCl 37 wt. % or NH_4OH 29 wt. %. Ethanol addition was performed using absolute ethanol (Sigma Aldrich). In all cases, the molar ratios of 1.36/n $(C_6H_{10}O_5)_n$: 11 NH_3 : 144 H_2O : 58 C_2H_6O : 28 HCl were maintained.

The behavior of the suspensions was monitored by optical microscopy using a Leica optical microscope, model DME (Germany), mounted with Leica EC3 camera was used.

2.3 Synthesis procedures of mesoporous materials

2.3.1 Solids with potato and corn starch

The synthesis under controlled conditions was carried out in a 250 ml two-necked balloon immersed in a glycerin bath and coupled to a reflux cooling tube. Potato or corn starch is used as directing agents of the structure and tetraethylorthosilicate as a source of silicon, which is added drop by drop. Final solid was obtained by centrifugation at 12000 rpm and successive washings with distilled water until reaching neutral pH. Finally, the solids were calcined in air flow at 5 K min^{-1} up to 823 K for 4 h to achieve the total starch elimination.

Depending on the inherent behavior of starch in the aqueous phase, the synthesis was divided into two main stages: (i) gelatinization and (ii) retrogradation. In the first stage, the procedure was carried out at 353 K and the influence of time was analyzed at 2, 4 and 18 h. Furthermore, the HCl or ethanol addition in the synthesis medium was investigated.

On the other hand, the importance of the retrogradation stage at 298 K and time of 2 and 14 h was studied.

The nomenclature used for the synthesized samples was Xtg/tr/HCl-Et, where X is P or C and refers to potato or corn starch, t is the time (hours) of ‘g’: gelatinization or ‘r’: retrogradation. HCl-Et indicates the addition of HCl or ethanol, respectively. In all cases, the molar ratio of the synthesized solids was TEOS: 1.36/n $(C_6H_{10}O_5)_n$: 11 NH_3 : 144 H_2O : 58 C_2H_6O : 28 HCl.

2.4 Physicochemical characterization of mesoporous solids

2.4.1 N_2 adsorption/desorption isotherms

Nitrogen adsorption–desorption isotherms were obtained at 77 K on a Quantachrome Autosorb (Micromeritics, USA) instrument. Previously, samples were outgassed at 523 K for 4 h under vacuum. The linear region of Brunauer–Emmet–Teller (BET) plots was used to calculate the specific surface area of the materials from nitrogen adsorption isotherms [51]. The pore volume was calculated assuming cylindrical pores and using the Barret, Joyner y Halenda (BJH) method [18, 52].

2.4.2 Transmission Electron Microscopy (TEM)

On the other hand, the morphology of the synthesized materials was studied by Transmission Electron Microscopy (TEM). For that, a JEOL microscope, model JEM-2100 Plus (Japan) was used. Samples were crushed in an agate mortar and dispersed in ethanol and ultrasound. Then, a drop of the dispersion was deposited on the grid. Bare Cu grids of 300 mesh were used. Measurements were made in HRTEM mode and using an acceleration voltage of 200 kV.

2.5 CO_2 capture

The CO_2 adsorption experiments were carried out in a continuous flow system. The sample (ca. 100 mg) was placed in a tubular quartz reactor of 5 mm i.d., which was placed inside an electrical furnace equipped with a temperature controller. Subsequently, the sample was dehydrated in an inert flow at 773 K during 6 h. After cooling the solid sample to 373 K, it was exposed to 25 ml min^{-1} of 30 % CO_2/He.

The effluent gases were continuously monitored by on-line mass spectrometry (Pfeiffer/Balzers Quadstar, QMI422, QME125, Germany). The signal m/e 44 which correspond to the main partition of carbon dioxide were registered though mass spectrometry. In addition, other signals as 2 (hydrogen), 4 (helium), 28 (nitrogen or carbon monoxide), 32 (oxygen) and 18 (water) were monitored.

A typical breakthrough curve shows the evolution of the concentration of the hydrocarbon at the reactor outlet. The amount of CO_2 adsorbed during the breakthrough experiments (adsorption capacity) was calculated as the difference between the area under the curve in a blank experiment and the area under the breakthrough curve. The equation employed was:

$$Q_{ads} = \frac{F}{W}\int (C_0 - C)dt \qquad \text{Eq. (2)}$$

where Q_{ADS} is the adsorbed CO_2 amount, F is the CO_2/He flow, C is the outlet CO_2 concentration, C_0 is the initial CO_2 concentration, and W is the mass of adsorbent.

3. RESULTS AND DISCUSSION

3.1 Physicochemical characterization of the structure directing agents

The final properties of the synthesized mesoporous silica could depend on the botanical species of structure directing agent source. Although the phytotomy is different, both starches presented a similar amylose content, being 23.78 ± 0.16 % for potato starch and 25.25 ± 0.11 % for corn starch. In addition, several techniques of physicochemical characterization of potato and corn starches were applied.

3.1.1 Morphology of starch granules

Starch grains have different shapes and characteristics depending on the plant species from which derived. Figure 1 shows the SEM images obtained for potato (Figure 1A) and corn starch (Figure 1B).

The potato starch is characterized by ellipsoidal granules with a distance through its axis of symmetry close to 40 μm, as well as spheres with an average diameter between 10 and 20 μm. This ovoidal or piriform morphology with smooth and homogeneous surface is typical of potato starch.

On the other hand, granule shape of corn starch is irregular, polygonal in the plane and are assumed irregular polyhedral in space with a size smaller than soluble starch, which varies between 5 and 35 μm. The hilum is the center of growth of the granule. The location of the hilum is concentric, which reveals a development of the equi-radial granule with the mentioned polyhedral imperfections.

3.1.2 Crystalline Structure

The XRD measurements of potato and corn starches are presented in Figure 2A. It is possible to observe the diffraction peaks corresponding to the crystalline fraction of starches overlapping a wide halo characteristic of amorphous fraction. Usually accepted model of a typical cereal

starch granule involves alternating amorphous and crystalline lamellae, in which the main two components, amylose and amylopectin are embedded.

According to several investigation, starch can be classified to A, B and C forms. In granular forms, the A pattern is associated mainly with cereal starches, while B form is usually obtained from tuber starches (Figure 2A). C-type form is a mixture of both A and B types, but also occurs naturally, e.g. smooth-seeded pea and various bean starches [53]. The main difference between A and B types is that the former adopts a close-packed arrangement with water molecules between each double helical structure, while the B-type is more open, there being more water molecules, essentially all of which are located in a central cavity surrounded by six double helices [54].

Potato starch showed diffraction peaks at 2θ = 14.6, 16.8, 19.1, 21.9, 23.6 and 25.6 degrees, demonstrating a B-type diffraction pattern, characteristic for the starch found in plant tubers (Figure 2A-a) [55, 56].

Instead, the diffraction pattern of corn starch showed diffraction peaks at 2θ = 14.6, 16.8, 17.5, 19.7 and 22.7 degrees, demonstrating a diffraction peak of A-type. This kind of crystalline packing forms a monoclinic type cell (Figure 2A-b) [57].

3.1.3 FTIR analysis

The IR spectra obtained for starches are shown in Figure 2B. In the region at 1850-600 cm^{-1} of the FTIR spectra, a broad band at 1657 cm^{-1} was assigned to hydroxyl groups form water molecules absorbed in the amylose regions of the starch granule. In addition, the band with a maximum at 1464 cm^{-1} is attributed to the bending vibration CH_2, while the band with the maximum at 1373 cm^{-1} is associated with C-O-H bending vibrations and twisting CH_2. The bands observed between 980 and 1050 cm^{-1} are related to the CO bond vibrations in the glucopyranose rings [58]. The bands between 930 and 600 cm^{-1} correspond to the skeletal vibrations of the α-1,4-glycosidic bonds. In these regions no appreciable differences are observed.

The most significant difference in the FTIR spectra between both starches, are the band at 1737 cm^{-1} that are presented in the potato starch. Hernández-Martínez et al. [59] reported the presence of ester group in the range of 1793-1693 cm^{-1} for soybean oil. In the same way, S. Jain and co-workers [60] investigated native and modified rice starch by FTIR. The region between 950 and 1800 cm^{-1} was referred as the fingerprint of starches with a complex spectrum. The differences in this area of the spectrum can be attributed to the vibrational state of the glucose unit of the starch monomer [61]. Modifications on the starches resulted in structural and physicochemical variations that lead to changes in the vibrations of the glucose molecule, resulting in differences in their FTIR spectra. The presence of a peak at 1724 cm^{-1} attributed to the vibration of the C=O bond of an ester group, confirming the formation of ester carbonyl groups and the substitution of octenyl succinic anhydride (OSA) on the samples of modified starch [62]. In this way, it is observed that the potato starch used for the synthesis contains ester groups unlike corn starch.

3.1.4 Thermogravimetric studies

Figure 3A shows the mass losses as a function of temperature obtained by TGA for potato and corn starches. The respective differential thermal analysis curves are plotted in Figure 3B. Three important zones are observed where the most pronounced weight losses are represented in the thermogravimetric analysis.

The first zone that occurs at temperatures below 373 K corresponding to physisorbed water [63] and represents a loss of 19 and 10 % for potato and corn starch, respectively. A second zone of thermal degradation that is in the range of 473 to 643 K, which corresponds to the decomposition of carbohydrates and low molecular weight components such as starch [64, 65]. The third zone that manifests itself above 643 K was observed only in potato starch and corresponds to the decomposition of higher molecular weight polysaccharides, among which are protein residues and lipids. Although in region 2 the potato and corn starches present a decomposition of 54 % and 79 %, respectively, significant differences are observed in the decomposition at high temperatures (zone 3). Potato starch shows a significant weight loss (22

%), while corn starch is almost negligible (5 %). The ash content is similar in both cases, being 6 % for corn starch and 5 % for potato starch.

It is important to bear in mind that for the synthesis of mesoporous SiO_2, the directing agent of the structure must be removed at the end of synthesis. Particularly, these results indicate that after the synthesis of mesoporous silica, both starches will be eliminated around 800 K.

3.2 Influence of the ethanol addition, pH and temperature in aqueous starch suspensions

The modification of starch grain morphology was studied by adjusting the temperature between 303 K and 353 K, different pH, with and without ethanol addition and following by optical microscopy.

3.2.1 *Study of pH influence*

Figure 4 presents de microscopic images obtained when the corn starch is in neutral (Figures 4A, 4B, 4C), basic (Figures 4D, 4E, 4F) and acid (Figures 4G, 4H, 4I) medium at different temperatures.

At room temperature, the granule of corn starch in neutral aqueous suspension (Figure 4A) has a polygonal shape and the typical malt cross, with homogeneous sizes close to 18.7 μm. In this context, it is important to note that starch granules are insoluble in water at room temperature. However, water can be absorbed in a reversible way due to their highly organized structure and great stability caused by the multiple interactions that exist with their two constituent polysaccharides [66]. When the suspension is heated to 323 K (Figure 4B), the morphology of the granules is maintained and the average size is 19.6 μm. This slight increase in grain size is associated with the beginning of the imbibition or water absorption in the amorphous intermicellar areas, which are the least organized and most accessible. In this zone, hydrogen bonds are not as numerous or rigid as in crystalline areas. As the temperature increases and 353 K is reached, more water is retained, the grain begins to swell and increases in volume as shown in Figure 4C. Once the amorphous fragment has been fully hydrated, the crystalline particles

initiates a similar process, but this requires more energy. In general, when starch is subjected to certain temperatures, the granule reaches its maximum volume and loses its crystallinity. Specifically in this case, the corn starch granule at 353 K loses its polygonal morphology and increases its size to a value close to 29.7 μm, due to the hydration of the grain. In addition, the image shows a smooth edge which indicates that there is no rupture of the granule.

On the other hand, when the suspension is basic, the morphology of the corn starch granule is similar to that in neutral conditions with increasing temperature. At 303 K, the starch grain presents the typical morphology of corn with an average size of 17.1 μm (Figure 4D). When the temperature increases to 323 K (Figure 4E), the grain maintains its morphology and even the malt cross, indicative of the non-absorption of water at this temperature. The average grain size is 17.0 μm. On the contrary, in Figure 4F it is observed that when 353 K is reached, the malt cross is lost, and the grain size increases to values close to 41.1 μm. The kinetic energy of hot water breaks the hydrogen bonds between the starch molecules. As hydrogen bonds are formed, the water has a greater ability to penetrate the granule and swelling and consequent enlargement of the grain occurs. This process is irreversible and occurs after reaching a critical or "gelatinization" temperature [67]. Therefore, the incorporation of NH_4OH to the solution promotes the absorption of water at 353 K, due to the fact that the grain size increases from 29.7 μm (Figure 4C) to 41.1 μm (Figure 4F). It is also observed that the grain does not have well-defined edges and presents roughness on the inside due to the beginning of the breakdown of the granules, where they release amylose and amylopectin chains that form the colloidal network. The breakdown of the starch grain is associated with the gelatinization process which, in this case, is promoted by the presence of ammonium hydroxide.

The most noticeable difference is seen when the medium is acidified with HCl. In Figure 4G the swelling of the starch grain at room temperature is shown, reaching an average size of 63.5 μm. In addition, the tortuous edges of the grain and the irregularity of its interior as a result of its rupture are highlighted. Thus, as the temperature increases to 323 and 353 K, the grain breaks down to sizes of 25.0 and 17.6 μm, respectively (Figure 4H and 4I). Consequently, it can be

highlighted that using an acid medium and low temperatures in the synthesis medium favors the gelatinization process, that is, the disintegration of the native granule structure [68].

A similar behavior is observed with potato starch. Figure 5 shows the images obtained with potato starch at neutral (Figures 5A, 5B and 5C), basic (Figures 5D, 5E and 5F) and acid (Figures 5G, 5H and 5I) pH at different temperatures. Starch suspension at room temperature (Figure 5A), presents ovoid or pyriform morphology typical of potato starch, with a heterogeneous grain size and close to 45.5 μm. At 323 K some small breaks in the grain stand out, indicated in Figure 5B. The swelling of the granule is observed once it reaches 353 K. Under these conditions the grain size increases to 87.5 μm (Figure 5C). With the NH_4OH addition, a similar trend is observed as in neutral conditions. As the temperature increases, the absorption of water and consequent swelling of the granule occurs. The main difference observed compared to the neutral medium is that the average grain size is larger as the firing progresses, being 57.9 μm and 102.5 μm at 323 K (Figure 5E) and 353 K (Figure 5F), respectively. This indicates that as with corn starch, the presence of NH_4OH promotes water absorption.

On the other hand, in an acid medium the main difference is observed. At room temperature (Figure 5G) the starch grain absorbs water, increasing its size to values close to 174.5 μm and observing the grain breakdown. Once cooking begins, the presence of starch grains is no longer visible (Figures 5H and 5I), probably due to its hydrolysis. Acid hydrolysis during cooking of starch granules results in the formation of dextrins or short chain polymers. The acid breaks down the starch molecule.

3.2.2 *Study of EtOH addition*

The study of EtOH influence is analyzed taking into account that in hydrothermal synthesis of MCM41 type mesoporous materials, ethanol is used as a co-solvent to favor the dilution of the surfactant in the aqueous medium [18, 69].

Following with the same line of analysis, Figures 6 and 7 show the microscopic images obtained for potato and corn starch, respectively, with the addition of ethanol, at different temperatures and pH.

When the synthesis medium is neutral, the potato starch grain size increases slightly as the cooking temperature increases. It reaches mean values of 39.0, 41.9 and 49.2 μm at 303, 323 and 353 K, respectively (Figure 6, microscopies A-C). At high temperatures, the potato starch grain does not absorb water or break down. Therefore, the evidence is clear that the addition of ethanol in neutral conditions delays the gelification process of potato starch. When the synthesis medium is basic (Figure 6, microscopies D-F), the starch grain swells only at 353 K, producing an increase in the size of the granule at values of 70.8 μm. Although water absorption occurs, the size achieved is 30 % lower than the value reported in the absence of ethanol. In the same vein, when the medium is acidic, a similar trend is observed. In the presence of ethanol at 353 K, the swelling of the granule is achieved with average values of 70.4 μm. However, the addition of ethanol inhibits acid hydrolysis towards lower molecular weight compounds. In this context, it can be observed that regardless of the medium pH and the synthesis temperature, the aggregation of ethanol retards the absorption of water and inhibits the gelling/hydrolysis processes.

In the case of corn starch (Figure 7), a different effect is observed compared to potato starch. In general terms, the sizes of the granules are maintained at different pH and temperatures, preserving the absorption and gelification processes.

As a summary of this section, it was observed that starch suspensions require a moderate temperature to promote water absorption by the grain, swelling and consequent hydration. When this process is irreversible, amylose and amylopectin chains are released as a consequence of the gelatinization process. Therefore, the temperature of 353 K (gelatinization temperature) was selected to carry out the silica synthesis as a consequence of the release of glucose units or short-chain polymers to be used as directing agents of the structure.

On the other hand, in both starches it was observed that the presence of ethanol delayed the gelation, as a consequence of dehydration process. Despite this, two solids were synthesized

with ethanol addition to verify this effect. In addition, the results suggest that the acidic medium would favor the breakage of the grain as a consequence of hydrolysis.

3.3 Synthesis of Mesoporous Materials

In this context, mesoporous silica samples were synthesized in neutral and acid aqueous medium, adding tetraethylorthosilicate (TEOS) as a source of silicon and potato or corn starches as directing agents of the structure. The silica materials obtained and the synthesis conditions selected are summarized in Table 1. During the synthesis, two stages of the starch are studied: (i) gelatinization at 353 K and times of 2, 4 and 18 h and in some cases and, (ii) starch retrogradation, lowering the temperature to 298 K and different times (2 and 14 h). Furthermore, the influence of ethanol addition and acidification of the synthesis medium with HCl solution was analyzed.

3.3.1 *Preparation with potato starch*

The textural properties were studied in order to characterize the porous structure of silica samples. Figure 8A shows the N_2 adsorption and desorption isotherms obtained at 77 K for the samples synthesized with potato starch considering only the gelatinization stage (Figure 8A-a), with retrogradation stage (Figure 8A-b) and finally, with the ethanol addition (Figure 8A-c). According to IUPAC classification, the isotherms obtained are type II which corresponds to non-porous or macroporous adsorbent solids. Table 2 shows the quantitative values of specific surface area, pore volume and pore diameter. P18 sample shows a surface area of 34.2 $m^2\ g^{-1}$, with a volume and average pore size of 0.09 $cm^3\ g^{-1}$ and 23.8 nm, respectively. When the starch retrogradation stage is considered, the textural properties are notably improved, reaching values of specific surface area of 130 $m^2\ g^{-1}$, pore volume of 0.49 $cm^3\ g^{-1}$ and average pore size of 22.5 nm. It is important to note that starch gelation occurs when water diffuses through the granule, then it swells substantially due to the hydration of its amorphous part [70, 71]. The gelation

process initially occurs in the amorphous region, favored by the weak hydrogen bonds present in this area. When starch granules swell and their components are in solution, the properties of the medium change from a simple starch suspension to a paste. Then, the retrogradation occurs when the paste generated in the gelation refrigerates [72]. During this process, amylose molecules associate with other glucose units to form a double helix, while amylopectin molecules recrystallize by assembly their small chains [73]. It is observed that for potato starch it is important to consider both stages of gelation and retrogradation to obtain a material with good textural properties.

On the other hand, the addition of ethanol in the synthesis medium produces a decrease in textural properties, such as the specific surface area and pore volume. In accordance with what was observed by optical microscopy, the addition of ethanol under neutral conditions delays the gelation process of potato starch, which directly influences in the textural properties of the material obtained.

In addition, Figure 8B shows the nitrogen adsorption and desorption isotherms by acidifying the synthesis medium. An IV-type isotherm typical of mesoporous materials with the appearance of the hysteresis cycle because of the mesoporous filling process is observed when 18 h and 353 K are used for the gelation stage and it is retrograded for 14 h at room temperature (Figure 8B-d). The hysteresis loop manifested is type-H2, typical of inorganic oxides such as silica [74]. Acidifying the synthesis medium, high values of the textural properties and representative of the mesoporous materials were obtained, with specific surface area, pore volume and average pore size of 639.3 m^2 g^{-1}, 0.28 cm^3 g^{-1} and 6.3 nm, respectively. The pore size distribution (PSD) is shown in Figure S1-A (Supplementary Data). In this way, the positive effect of the HCl addition during the synthesis is highlighted (Table 2). As observed with optical microscopy (Section 3.2.1), the presence of hydrochloric acid promotes the gelatinization stage, generating grain rupture as a consequence of acid hydrolysis.

In this context, the gelatinization time was reduced to 4 h and kept the rest of the conditions constant. In this case, Figure 8B-e shows the N_2 adsorption and desorption isotherm of

P4/14/HCl sample, which is type-IV with a hysteresis loop type-H2, representative of a mesoporous material with high surface specific area (708.6 m^2 g^{-1}), pore volume (0.38 cm^3 g^{-1}) and average pore size (3.9 nm). Therefore, by reducing the gelatinization time and acidifying the medium, the mesoporous material with the highest specific surface area is obtained. The pore size distribution is shown in Figure S1-A (Supplementary Data).

Finally, the influence of the retrogradation stage was analyzed by decreasing time from 14 to 2 h. Figure 8B-f display that P18/2/HCl sample shows a behavior similar to that of the P18/14 solid, where the adsorption and desorption isotherm obtained is type II corresponding to non-porous materials, with a specific surface area of 350.8 m^2 g^{-1} (Table 2). The PSD is shown in Figure S1-A (Supplementary Data). Therefore, the behavior could be attributed to the porosity caused by the interparticle space, as a consequence of nanoparticles packing, that is, a secondary mesoporosity.

Consequently, it is important to highlight that both retrogradation stage and synthesis in an acid medium are two key aspects to obtain mesoporous materials with good textural properties.

On the other hand, in order to analyze the morphology obtained for more relevant samples, Figures 9 and 10 show TEM images obtained for calcined P18/14 and P4/14/HCl samples, respectively.

Clear differences in TEM images are observed. On one hand, the sample with low surface area (P18/14) presents agglomerated and interconnected spherical nanoparticles and not well defined, with an average size between 10 and 20 nm (Figure 9). The packing of nanoparticles leaves hollow spaces, generating inter-particles mesoporosity that is, a secondary mesoporosity. These results agree with what was observed from the adsorption and desorption isotherms of N_2.

On the other hand, P4/14/HCl sample with a specific area of 708.6 m^2 g^{-1} presents a homogeneous spherical morphology with an average particle size close to 30 nm and a more defined porous structure (Figure 10) in concordance with the nitrogen adsorption and desorption isotherms.

3.3.2 *Preparation with corn starch*

In order to compare the results obtained with potato starch with other botanical source, samples were prepared using corn starch under the same synthesis conditions. Figure 11 and Table 3 show the N_2 adsorption and desorption isotherms and quantitative values of the textural properties obtained when corn starch was used as the structure directing agent.

Similar behavior to that reported when the synthesis is carried out with potato starch is observed. C18/14, C18 and C18/14/Et samples show a type II isotherm typical of non-porous materials (Figure 11A). It should be noted that C18/14 sample presented a surface area of 310.1 $m^2\ g^{-1}$, probably due to the presence of a secondary mesoporosity generated by the interparticle space, as occurred with potato starch.

Analyzing the isotherms obtained when the synthesis is performed in an acid medium, type IV isotherms are observed, typical of mesoporous materials (Figure 11B). In addition, C4/14/HCl sample presented excellent textural properties, reporting a specific surface area of 1018.1 $m^2\ g^{-1}$, pore volume of 0.15 $cm^3\ g^{-1}$, and an average pore size of 5.6 nm. The pore size distribution is shown in Figure S1-B (Supplementary Data). Significant improvement in surface area and pore volume was observed in all samples. Therefore, it is important to highlight the importance of HCl to promote starch hydrolysis during mesoporous silica synthesis, regardless of the botanical source of the structure-directing agent.

Figure 12 presents TEM images obtained for C4/14/HCl sample. Uniform spherical morphology with a homogeneous diameter close to 300 nm is observed. In addition, the presence of regular pores is hinted at in agreement with the results observed through N_2 adsorption and desorption.

3.3.3 *Comparison of samples synthesized with starches and CTAB*

Mesoporous MCM41 synthesis was reported previously by our group [18, 23, 71]. For that, n-hexadecyltrimetilammonium bromide (CTAB) was used as template. The N_2 adsorption and desorption isotherms obtained for this material was type IV according to the IUPAC classification, which are typical of mesoporous materials [18, 75, 76], with a strong inflection at

relative pressures p/p° > 0.3, which indicates the uniformity of the mesoporous size distribution. The MCM41 sample showed a surface area and pore volume values of 1295 cm^2 g^{-1} and 0.39 cm^3 g^{-1}, respectively. Thus, the values obtained using potato and/or corn starch are similar and representative of a mesoporous silica such as MCM41. On the other hand, the TEM images corresponding to MCM41 sample showed a spherical morphology with mean size close to 500 nm [75-77]. Instead, mesoporous materials synthesized with CTAB as a surfactant are identified as mesoporous silicas that present a one-dimensional cylindrical pore packing in a hexagonal assembly [76]. This arrangement is characteristic of these materials and occurs because aqueous solutions of the quaternary cationic surfactant CTAB are used in the preparation and consequent formation of micelles.

In comparison to starches, they do not have the ability to form micelle, so the materials obtained do not present a defined order as observed by small-angle X-ray scattering. The generated mesoporosity has a random order defined by the arrangement of the starch and the generated bonds.

It is observed that the results obtained using both potato and corn starch are comparable with samples synthesized with CTAB surfactant and are promising and encourage further study.

3.4 Mechanism of synthesis

It is important to reach a global understanding of the synthesis mechanism, in order to advance in the area of mesoporous materials synthesis using natural structure directing agents. Until now, mesoporous solids with high specific surface area and good textural properties have been obtained considering the starch gelatinization and retrogradation stage and acidifying the synthesis medium.

Considering the results obtained, a scheme of reactions that occur during the synthesis in acid medium is proposed in Figure 13. For this, the first stage of starch solubility and gelation and the second of retrogradation are considered. Certainly, under acidic conditions at 353 K, a first

stage occurs which consists of acid hydrolysis of starch and alkoxide (TEOS). In the case of TEOS, a colloidal suspension is obtained while the silanol groups (Si-OH) are formed and ethanol is released [78]. Simultaneously, potato or corn starch molecules depolymerize or break bonds randomly, producing smaller fragments corresponding to their monosaccharide such as glucose. The hydroxonium ion attacks the oxygen in the glycosidic bond and then hydrolyzes the bond. The degree of hydrolysis depends on time. In this case, it has been shown that 4 h were enough to obtain solid materials with the expected properties. Then, the binding mechanism of glucose with hydrolyzed TEOS corresponds to a SN2 nucleophilic substitution on the Si atom [79].

When the synthesis temperature is lowered to 298 K, condensation reactions of the hydrolyzed TEOS and glucose are promoted. The polymerization of the silanol groups forms structures linked by siloxane bonds (Si-O-Si) with remove of water and ethanol. It should be noted that there is no cationic surfactant in the synthesis medium that promotes the formation of micelles and consequent mesoporous ordering thus, there is a significant fraction of silanol groups that polymerize without ordering. On the other hand, monosaccharides such as glucose join to form disaccharides through the condensation reaction itself. In this way, from the association of two glucose molecules (bound to the hydrolyzed TEOS) disaccharides are formed (releasing a water molecule) which, when eliminated by calcination, leave holes that correspond to the observed pores.

Then, it can be summarized that the presence of acid is important, to promote the hydrolysis of the silicon source and the starches used. In addition, it is essential to increase the temperature during hydrolysis to further promote starch solubilization and, finally, lower the temperature to carry out the condensation and polymerization stage. Finally, all the materials are calcined in air flow to stabilize the material, eliminating the starch present.

3.5 CO_2 capture at low temperature

Silica-based mesoporous materials are widely used in low-temperature CO_2 adsorption processes. Therefore, the materials synthesized with starch and better textural properties were

evaluated in CO_2 adsorption at 373 K and compared with the reference solid MCM41 synthesized with CTAB.

In this sense, the determination of rupture or breakthrough curves is a direct method used to determine the adsorption capacity of adsorbent materials. Figure 14 compares breakthrough curves for carbon dioxide adsorption at 373 K on MCM41 sample and those synthesized with potato and corn starches. In addition, CO_2 adsorbed amount (Q_{ads}) and the ratio between Q_{ads} per specific surface area are presented in Table 4.

The reference material MCM41 synthesized with CTAB, presents an adsorption capacity of 168.6 mg CO_2 g_{ads}^{-1}. The materials prepared with potato or corn starches in an acid medium showed comparative values with an adsorption capacity between 37.0 and 150.2 mg CO_2 g_{ads}^{-1}. Table 4 show the CO_2 adsorbed amount linked to the specific surface area thus, the adsorbent solid behavior strongly depends on the textural properties achieved. It stands out that the solid P18/14/HCl is the one that presented the highest amount of CO_2 adsorbed per surface, reporting a ratio value of 0.22 mg CO_2 m^{-2}. All the materials synthesized with potato or corn starches in an acidic medium and with high condensation times (14 h) presented higher amounts of adsorption per specific surface than the reference solid MCM41.

When comparing these results with those reported in the open literature, mesoporous materials based on SBA-15 and functionalized with different contents of amine groups to promote carbon dioxide adsorption are observed. Callejas et al. [48] reported CO_2 adsorption values with solid SBA-15 of 19.7 mg CO_2 m^{-2} at 318 K, indicating a ratio of 0.03 mg CO_2 m^{-2}. After functionalizing it with high contents of polyethyleneimine (PEI) (30 and 50 wt. %), the amount of adsorbed CO_2 increased to 60.8 and 75.0 mg CO_2 g^{-1}, respectively. Reasonably, when high PEI contents were incorporated, the specific surface area decreases, the ratio between the amount adsorbed and the available area increases to 0.40 and 1.53 mg CO_2 m^{-2} for SBA-PEI(30) and SBA-PEI(50), respectively. When the amine-type was changed and functionalizing with 10 wt. % of diethylenetriaminopropyl (DT-NNN), the material adsorbed 80.0 mg CO_2 g^{-1}, which

indicates 0.98 mg CO_2 m^{-2} [80]. It is important to highlight that these adsorption results were obtained at a lower temperature.

In this way, it is observed that CO_2 adsorption values obtained with non-functionalized mesoporous silica and synthesized with potato or corn starch present values comparable to those currently reported in the available literature.

Thus, it can be seen that it is possible to synthesize a mesoporous silica-based material in random order using a natural structure-directing agent such as starch. It is not minor to take into account that the results can be extrapolated to starches from different botanical sources.

4. CONCLUSIONS

Mesoporous silica with specific surfaces area of 708.60 and 1018.10 m^2 g^{-1} were synthesized using potato and corn starch as directing agent of the structure, respectively. The stages of starch gelatinization and retrogradation are necessary to achieve materials with good textural properties. In addition, the optimal synthesis conditions are linked to the acidification of the medium to promote the hydrolysis of starch into its monomeric units (glucose) and subsequent S_N2 nucleophilic substitution process to interact with the silicon source. The presence of ethanol in the synthesis medium is not favorable due to the dehydration process that leads to delayed starch solubility and gelation.

The most promising material obtained showed a CO_2 adsorption capacity of 0.22 mg CO_2 m^{-2} at 373 K. These values are close to those synthesized with the commercial CTAB surfactant.

Starches from different botanical sources but similar physicochemical properties led to the synthesis of mesoporous silica with similar synthesis conditions and textural properties. In this way, it is possible to predict and extrapolate the synthesis conditions to different starches used as directing agents of the structure.

ACKNOLEDGEMENTS

The authors acknowledge the financial support received from UNL (CAID 50620190100102LI), ANPCyT (PICT 2019-00422) and CONICET (PIP 11220200100607CO).

Thanks are given to Yohana Martínez for the TEM measurements.

REFERENCES

[1] V. Jancikova, M. Jablonsky, Fractionation of Biomass using Green Solvents, Biointerface Research App. Chem. 13 (2023) 261. http://dx.doi.org/10.33263/BRIAC133.261

[2] S. Pan, H.M. Zabed, Y. Wei, X. Qi, Technoeconomic and environmental perspectives of biofuel from sugarcane bagasse: Current status, challenges and future outlook, Ind. Crops Prod. 188 (2022) 115684. https://doi.org/10.1016/j.indcrop.2022.115684

[3] M.C. Pereira Gonçalves, P.J. Romanelli, A.B. Moulin Cansian, E.F. Queiroz Pucci, J.R. Guimarães, P. Waldir Tardioli, B.A. Saville, A review on the production and recovery of sugars from lignocellulosics for use in the synthesis of bioproducts, Ind. Crops Prod. 186 (2022) 115213. https://doi.org/10.1016/j.indcrop.2022.115213

[4] M. Barbosade Farias, P. Prediger, M. Gurgel, A. Vieira, Conventional and Green-synthesized nanomaterials applied for the adsorption and/or degradation of phenol: A recent overview, J. Cleaner Prod. 367 (2022) 132980. https://doi.org/10.1016/j.jclepro.2022.132980

[5] A. Ullah, S.I. Lim, Plant extract-based synthesis of metallic nanomaterials, their applications, and safety concerns, Biotechn. Bioeng. 119 (2022) 2273-2304. https://doi.org/10.1002/bit.28148

[6] B. Ngayakamo, A.P. Onwualu, Recent advances in green processing technologies for valorization of eggshell waste for sustainable construction materials, Heliyon 8 (2022) e09649. https://doi.org/10.1016/j.heliyon.2022.e09649

[7] T.A. Wani, G. Suresh, Plant-Mediated Green Synthesis of Magnetic Spinel Ferrite Nanoparticles: A Sustainable Trend in Nanotechnology, Adv. Sust. System 6 (2022) 2200035. https://doi.org/10.1002/adsu.202200035

[8] S.A. Yamada, S.T. Hung, W.H. Thompson, M.D. Fayer, Effects of pore size on water dynamics in mesoporous silica. J. Chem. Phys. 152 (2020) 154704. https://doi.org/10.1063/1.5145326

[9] M. Wu, L. Shi, T-T. Lim, A. Veksha, F. Yu, H. Fan, J. Mi, Ordered mesoporous Zn-based supported sorbent synthesized by a new method for high-efficiency desulfurization of hot coal gas. Chem. Eng. J. 353 (2018) 273-287. http://dx.doi.org/10.1016/j.cej.2018.07.134

[10] K. Hori, T. Higuchi, Y. Aoki, Effect of pore size, aminosilane density and aminosilane molecular length on CO_2 adsorption performance in aminosilane modified mesoporous silica, Microp. Mesop. Mater. 246 (2017) 158-165. https://doi.org/10.1016/j.micromeso.2017.03.020

[11] G. Zhao, T.S. Zhao, J. Xu, Z. Lin, X. Yan, Impact of pore size of ordered mesoporous carbon FDU-15-supported platinum catalysts on oxygen reduction reaction, Int. J. Hydr. En. 42 (2017) 3325-3334. https://doi.org/10.1016/j.ijhydene.2016.11.089

[12] Y. He, J. Li, M. Long, S. Liang, H. Xu, Tuning pore size of mesoporous silica nanoparticles simply by varying reaction parameters, J. Non-Cryst. Sol. 457 (2017) 9-12. https://doi.org/10.1016/j.jnoncrysol.2016.11.023

[13] Z. Wu, J. Sun, Y. Miao, E. Lei, Y. Liu, Z. Xu, K. Zhang, C. Ma, S. Luo, W. Li, S. Liu, Ordered mesoporous carbons from liquefied Wood: Morphological effects of nucleation and

growth processes, Chem. Eng. Sc. 264 (2022) 118094. https://doi.org/10.1016/j.ces.2022.118094

[14] T. Hua, D. Li, X. Li, J. Lin, J. Niu, J. Cheng, X. Zhou, Y. Hu, Synthesis of mesoporous-structured MIL-68(Al)/MCM-41-NH_2 for methyl orange adsorption: Optimization and Selectivity, Env. Research 215 (2022) 114433. https://doi.org/10.1016/j.envres.2022.114433

[15] A. Kaur, B. Bajaj, A. Kaushik, A. Saini, D. Sud, A review on template assisted synthesis of multi-functional metal oxide nanostructures: Status and prospects, Mat. Sc. Eng. B 286 (2022) 116005. https://doi.org/10.1016/j.mseb.2022.116005

[16] Y. Wu, X. Sun, X. Wang, J. Shen, Y. Ke, Pore size control of monodisperse mesoporous silica particles with alkyl imidazole ionic liquid templates for high performance liquid chromatograph applications, Colloids Surf. A: Physicochem. Eng. Asp. 637 (2022) 128200. https://doi.org/10.1016/j.colsurfa.2021.128200

[17] S-Y. Lee, S-M. Yoo, H.J. Lee, Adsorption and Cation-Exchange Behavior of Zinc Sulfide on Mesoporous TiO_2 Film and Its Applications to Solar Cells. Langmuir 36 (2020) 4144-4152. https://doi.org/10.1021/acs.langmuir.0c00095

[18] S.G. Aspromonte, A.V. Boix, Improving of cold-start and combustion emissions in lean NO conditions with active and selective AgAl mesoporous catalysts. J. Env. Chem. Eng. 7 (2019) 102995. https://doi.org/10.1016/j.jece.2019.102995

[19] J.S. Beck, J.C. Vartuli, W.J. Roth, M.E. Leonowicz, C.T. Kresge, K.D. Schmitt, C.T.W. Chu, D.H. Olson, E.W. Sheppard, S.B. McCullen, J.B. Higgins, J.L. Schlenker, A New Family of Mesoporous Molecular Sieves Prepared with Liquid Crystal Templates, J. Am. Chem. Soc. 114 (1992) 10834-10843. https://doi.org/10.1021/ja00053a020

[20] V. Alfredsson, H. Wennerström, The dynamic association processes leading from a silica precursor to a mesoporous SBA-15 material, Acc. Chem. Res. 48 (2015) 1891-1900. https://doi.org/10.1021/acs.accounts.5b00165

[21] B. Lu, Z. Wu, L. Ma, X. Yuan, Phosphotungstic acid immobilized on sulphonic-acid-functionalized SBA-15 as a stable catalyst for the esterification of cyclohexane with formic acid, J. Taiwan Inst. Chem. Eng. 88 (2018) 1-7. https://doi.org/10.1016/j.jtice.2018.03.021

[22] A. Lacoste, I. Tiscornia, A. Boix, CO preferential oxidation on cordierite monoliths coated with CuO-CeO_2/SBA-15 catalysts. Further insights into the physicochemical aspects of the catalytic behavior, Int. J. Hydrog. En. 43 (2018) 14238-14251. https://doi.org/10.1016/j.ijhydene.2018.05.122

[23] S.G. Aspromonte, M.D. Mizrahi, E. Alonso, J.M. Ramallo-López, A.V. Boix, Co/MCM41 catalyst in the COProx reaction prepared by supercritical CO_2 reactive deposition, Microp. Mesop. Mater. 239 (2017) 147-157. https://doi.org/10.1016/j.micromeso.2016.10.006

[24] C. Bernal, M. Mesa, M. Jaber, J.L. Guth, L. Sierra, Contribution to the understanding of the formation mechanism of bimodal mesoporous MCM41-type silica with large defect cavities. Microp. Mesop. Mater. 153 (2012) 217-226. https://doi.org/10.1016/j.micromeso.2011.12.049

[25] S. Che, Z. Liu, T. Ohsuna, K. Sakamoto, O. Terasaki, T. Tatsumi, Synthesis and characterization of chiral mesoporous silica, Nature 429 (2004) 281-284. https://doi.org/10.1038/nature02529

[26] M. Jensen, R. Keding, T. Höche, Y. Yue, Biologically formed mesoporous amorphous silica, J. Am. Chem. Soc. 131 (2009) 2717-2721. https://doi.org/10.1021/ja808847y

[27] K.M. Hawkins, S.S. Wang, D.M. Ford, D.F. Shantz, Poly-L-Lysine templated silicas: using polypeptide, J. Am. Chem. Soc. 126 (2004) 9112-9119. https://doi.org/10.1021/ja049936o

[28] H.K. Baca, C. Ashley, E. Carnes, D. Lopez, J. Flemming, D. Dunphy, S. Singh, Z. Chen, N. Liu, H. Fan, G.P. López, S.M. Brozik, M. Werner-Washburne, C.J. Brinker, Cell-directed

assembly of lipid-silica nanostructures providing extended cell viability, Science 313 (2006) 337-341. https://doi.org/10.1126/science.1126590

[29] M. Mizutani, H. Takase, N. Adachi, T. Ota, K. Daimon, Y. Hikichi, Porous ceramics prepared by mimicking silicified wood, Sci. Techn. Adv. Mater. 6 (2005) 76-83. https://doi.org/10.1016/j.stam.2004.08.004

[30] H.S. Zhao, W. He, Y.J. Feng, X.T. Jia, X.D. Zhang, Z.M. Li, S.P. Yan, W.J. Zhou, Biomimetic synthesis and characterization of magnetic proteins (magnetoferritin). Chem. Eng. Techn. 30 (2007) 1010-1013. https://doi.org/10.1002/ceat.200700104

[31] X. Zhang, G. Xu, H. Wang, H. Cui, X. Zhang, X. Wang, Enhanced acetone sensing properties of hollow SnO_2 fibers using poplar catkins as a bio-template, Powder Techn. 344 (2019) 183-189. https://doi.org/10.1016/j.powtec.2018.12.020

[32] Y. Ma, Q. Wei, R. Ling, F. An, G. Mu, Y. Huang, Synthesis of macro-mesoporous alumina with yeast cell as bio-template, Microp. Mesop. Mater. 165 (2013) 177-184. https://doi.org/10.1016/j.micromeso.2012.08.016

[33] B. Zhang, S.A. Davis, S. Mann, Starch gel templating of sponge like macroporous silicalite monoliths and mesoporous films, Chem. Mater. 14 (2002) 1365-1369. https://doi.org/10.1007/978-3-319-32101-1_127

[34] Y. Liu, T.J. Pinnavia, Aluminosilicate nanoparticles for catalytic hydrocarbon cracking, J. Am. Chem. Soc. 125 (2003) 2376-2377. https://doi.org/10.1021/ja029336u

[35] Y. Liu, W. Zhang, Z. Liu, S. Xu, Y. Wang, Z. Xie, X. Han, X. Bao, Direct observation of the mesoporos in ZSM5 zeolites with hierarchical porous structures by laser hyperpolarized ^{129}Xe NMR. J. Phys. Chem. C 112 (2008) 15375-15381. https://doi.org/10.1021/jp802813x

[36] L. Wang, C. Yin, Z. Shan, S. Liu, Y. Du, F. Xiao, Bread-template synthesis of hierarchical mesoporous ZSM-5 zeolite with hydrothermally stable mesoporosity, Coll. Surf. A Physicochem. Eng. Asp. 340 (2009) 126-130. https://doi.org/10.1016/j.colsurfa.2009.03.013

[37] X. Yang, T. Lu, C. Chen, L. Zhou, F. Wang, Y. Su, Synthesis of hierarchical AlPO-n molecular sieves templated by saccharides, Microp. Mesop. Mater. 144 (2011) 176-182. https://doi.org/10.1016/j.micromeso.2011.04.011

[38] H. Tao, C. Li, J. Ren, Y. Wang, G. Lu, Synthesis of mesoporous zeolite single crystals with cheap porogens, J. Solid State Chem. 184 (2011) 1820-1827. https://doi.org/10.1016/j.jssc.2011.05.023

[39] W. Lai, L. Pang, J. Zheng, J. Li, Z. Wu, X. Yi, Efficient one pot synthesis of mesoporous NiMo-Al_2O_3 catalysts for dibenzothiophene hydrodesulfurization, Fuel Process. Technol. 110 (2013) 8-16. https://doi.org/10.1016/j.fuproc.2013.01.006

[40] V.N. Stathopoulos, T. Kuznetsova, O. Lapina, D. Khabibulin, P.K. Pandis, T. Krieger, Y. Chesalov, R. Gulyalev, V. Krivensov, T. Larina, V. Sadykov, Evolution of bulk and surface structures in stoichiometric $LaAlO_3$ mixed oxide prepared by using starch as template, Mat. Chem. Phys. 207 (2018) 423-434. https://doi.org/10.1016/j.matchemphys.2017.12.056

[41] S. Ren, C. Gong, P. Zeng, Q. Guo, B. Shen, Synthesis of flammulina-like moredenite using starch as template and high catalytic performance in crack of wax oil. Fuel 166 (2016) 347-351. https://doi.org/10.1016/j.fuel.2015.11.010

[42] T.R. Karl, K.E. Trenberth, Modern Global Climate Change, Science 302 (2003) 1719-1723. https://doi.org/10.1126/science.1090228

[43] Carbon Dioxide Information Analysis Center (CDIAC) https://cdiac.ess-dive.lbl.gov.

[44] C. Mora, A.G. Frazier, R.J. Longman, R.S. Dacks, M.M. Walton, E.J. Tong, J.J. Sanchez, L.R. Kaiser, Y.O. Stender, J.M. Anderson, C.M. Ambrosino, I. Fernández-Silva, L.M. Giuseffi,

T.W. Giambelluca, The projected timing of climate departure from recent variability, Nature 502 (2013) 183-187. https://doi.org/10.1038/nature12540

[45] R. Das, S.S. Dhankhar, C.M. Nagaraja, Construction of a bifunctional Zn(II)-organic framework containing a basic amine functionality for selectivity capture and room temperature fixation of CO_2, Inorg. Chem. Front. 7 (2020) 72-81, https://doi.org/10.1039/C9QO01058K

[46] M.S.B. Reddy, D. Ponnamma, K.K. Sadasivuni, B. Kumar, A.M. Abdullah, Carbon dioxide adsorption based on porous materials, RCS Adv. 11 (2021) 12658-12681, https://doi.org/10.1039/d0ra10902a

[47] R. Sanz, G. Calleja, A. Arencibia, E.S. Sanz-Pérez, CO_2 capture with pore-expanded MCM-41 silica modified with amino groups by double functionalization. Microp. Mesop. Mater. 209 (2015) 165-171. https://doi.org/10.1016/j.micromeso.2014.10.045

[48] R. Sanz, G. Calleja, A. Arencibia, E.S. Sanz-Pérez, Amino functionalized mesostructured SBA-15 silica for CO_2 capture: Exploring the relation between the adsorption capacity and the distribution of amino groups by TEM, Microp. Mesop. Mater. 158 (2012) 309-317. https://doi.org/10.1016/j.micromeso.2012.03.053

[49] E.S. Sanz-Pérez, A. Arencibia, G. Calleja, R. Sanz, Tuning the textural properties of HMS mesoporous silica. Functionalization towards CO_2 adsorption. Microp. Mesop. Mater. 260 (2018) 235-244. https://doi.org/10.1016/j.micromeso.2017.10.038

[50] B. Belhadi, D. Djabali, R. Souilah, M. Yousfi, B. Nadjemi, Three small-scale laboratory steeping and wet-milling procedures for isolation of starch from sorghum grains cultivated in Sahara of Algeria, Food and Bioproducts Processing 91 (2013) 225-232. https://doi.org/10.1016/j.fbp.2012.09.008

[51] B. Lippens, B. Linsen, J. de Boer, Studies on pore systems in catalysts. The t method, J. Catal. 3 (1964) 32–37. https://doi.org/10.1016/0021-9517(65)90307-6

[52] S.G. Aspromonte, F.A. Piovano, O. Sánz, A.V. Boix, E. Alonso, Valorization of the wheat bran C5 fraction using Ru/ZrO2-MCM48 catalysts, ACS Sust. Chem. Eng. 10 (2022) 16324-16334. https://doi.org/10.1021/acssuschemeng.2c05412

[53] N.W.H. Cheetham, L. Tao, Variation in crystalline type with amylose content in maize starch granules: an X-ray powder diffraction study, Carbohydr. Polym. 36 (2018) 277-284. https://doi.org/10.1016/S0144-8617(98)00007-1

[54] K. Kaczmarska, B. Grabowska, T. Spychaj, M. Zdanowicz, M. Sitarz, A. Bobrowski, S. Cukrowicz, Effect of microwave treatment on structure of binders based on sodium carboxymethyl starch: FT-IR, FT-Raman and XRD investigations, Spectrochim. Acta Part A: Mol. Biomol. Spectr. 199 (2018) 387-393. https://doi.org/10.1016/j.saa.2018.03.047

[55] G. Lewandowicz, J. Fornal, A. Walkowski, Effect of microwave radiation on physico-chemical properties and structure of potato and tapioca starches, Carbohydr. Polym. 34 (1997) 213-220. https://doi.org/10.1016/S0144-8617(97)00091-X

[56] P. Ambigaipalan, R. Hoover, E. Donner, Q. Liu, Retrogradation characteristics of pulse starches, Food Res. Int. 54 (2013) 203-212. https://doi.org/10.1016/j.foodres.2013.06.012

[57] M-N- Li, Y. Xie, H-Q. Chen, B. Zhang, Effects of heat-moisture treatment after citric acid esterification on structural properties and digestibility of wheat starch, A- and B-type starch granules, Food Chem. 272 (2019) 523-529. https://doi.org/10.1016/j.foodchem.2018.08.079

[58] O. Anjos, M.C. Campos, P. Contreras Ruiz, P. Antunes, Application of FTIR-ATR spectroscopy to the quantification of sugar in honey, Food Chem. 169 (2015) 218-223. https://doi.org/10.1016/j.foodchem.2014.07.138

[59] M. Hernández-Martinez, T. Gallardo-Velázquez, G. Osorio-Revilla, Rapid characterization and identification of fatty acids in margarines using horizontal attenuate total reflectance

Fourier transform infrared spectroscopy (HATR-FTIR), Eur. Food Research Techn. 231 (2010) 321-329. https://doi.org/10.1007/s00217-010-1284-9

[60] S. Jain, T. Winuprasith, M. Suphantharika, Design and synthesis of modified and resistant starch-based oil-in-water emulsions, Food Hydrocol. 89 (2019) 153-162. https://doi.org/10.1016/j.foodhyd.2018.10.036

[61] R. Kizil, J. Irudayaraj, J. Seetharaman, Characterization of irradiated starches by using FT-Raman and FTIR spectroscopy, J. Agr. Food Chem. 50 (2002) 3912-3918. https://doi.org/10.1021/jf011652p

[62] M. Sharma, A.K. Singh, D.N. Yadav, Rheological properties of reduced fat ice cream mix containing octenyl succinylated pearl millet starch, J. Food Sc. Techn. 54 (2017) 1-8. https://doi.org/10.1007/s13197-016-2359-9

[63] S. Ek, A. Root, M. Peussa, L. Niinistö, Determination of the hydroxyl group content in silica by thermogravimetry and a comparison with 1H MAS NMR results, Thermochim. Acta 379 (2001) 201-212. https://doi.org/10.1016/S0040-6031(01)00618-9

[64] Y. Liu, A. Liu, S. Ibrahim, H. Yang, Isolation and characterization of microcrystalline cellulose from pomelo peel, Int. J. Biol. Macromol. 111 (2018) 717-721. https://doi.org/10.1016/j.ijbiomac.2018.01.098

[65] S. Ventura-Cruz, N. Flores-Alamo, A. Tecante, Preparation of microcrystalline cellulose from residual Rose stems (Rosa spp.) by successive delignification with alkaline hydrogen peroxide, Int. J. Biol. Macromol. 155 (2020) 324-329. https://doi.org/10.1016/j.ijbiomac.2020.03.222

[66] V. Espinosa-Solis, J.L. Jane, L.A. Bello-Perez, Physicochemical characteristics of starches from unripe fruits of mango and banana, Starch/Stärke 61 (2009) 291-299. https://doi.org/10.1002/star.200800103

[67] R.A. Freitas, R.C. de Paula, J.P.A. Feitosa, S. Rocha, M.R. Sierakowski, Amylose contents, rheological properties and gelatinization kinetics of yam (Dioscorea alata) and cassava (Manihot utilissima) starches, Carbohydr. Polym. 55 (2016) 3-8. https://doi.org/10.1016/S0144-8617(03)00142-5

[68] M. Schirmer, M. Jekle, T. Becker, Starch gelatinization and its complexity for analysis, Starch/Stärke 67 (2015) 30-41. https://doi.org/10.1002/star.201400071

[69] S.G. Aspromonte, M.D. Mizrahi, E. Alonso, J.M. Ramallo-López, A.V. Boix, Co/MCM41 catalyst in the COProx reaction prepared by supercritical CO_2 reactive deposition, Microp. Mesop. Mater. 239 (2007) 147-157. https://doi.org/10.1016/j.micromeso.2016.10.006

[70] J.P.J. Jenkins, R.E. Cameron, A.M. Donald, A universal feature in the structure of starch granules from different botanical sources, Starch/Stärke 45 (1993) 417-420. https://doi.org/10.1006/jcrs.2001.0374

[71] A. Jiménez, M.J. Fabra, P. Talens, A. Chiralt, Edible and biodegradable starch films: a review, Food Bioproces. Techn. 5 (2012) 2058-2076. https://doi.org/10.1007/s11947-012-0835-4

[72] R. Hoover, Acid-treated starches. Food Rev. Int. 16 (2000) 369-392. https://doi.org/10.1081/FRI-100100292

[73] N. Singh, J. Singh, L. Kaur, N. Singh Sodhi, Morphological Thermal and rheological properties of starches from different botanical sources, Food Chem. 79 (2003) 183-192. https://doi.org/10.1016/S0308-8146(02)00130-9

[74] M. Bourebrab, D.T. Oben, G. Durand, P.G. Taylor, Influence of the initial chemical conditions on the rational design of silica particles, J. Sol-Gel Sc. Techn. 88 (2018) 1-12. https://doi.org/10.1007/s10971-018-4821-9

[75] S.G. Aspromonte, A. Sastre, A.V. Boix, M.J. Cocero, E. Alonso, Cobalt oxide nanoparticles on mesoporous MCM-41 and Al-MCM-41 by supercritical CO_2 deposition Microp. Mesop. Mater. 148 (2012) 53-61. https://doi.org/10.1016/j.micromeso.2011.07.014

[76] S. Aspromonte, A. Sastre, A. Boix, M.J. Cocero, E. Alonso, Optimization and modelling of the supercritical CO_2 deposition of Co_xO_y nanoparticles on MCM41 supports, J. Sup. Fluids 110 (2016) 47-55. https://doi.org/10.1016/j.supflu.2015.11.026

[77] S.G. Aspromonte, F.A. Piovano, E. Alonso, A.V. Boix, Synthesis of supported mesoporous catalysts using supercritical CO_2, in Advances in Microporous and Mesoporous Materials, London, United Kingdom: IntechOpen, (2020) [Online]. doi:10.5772/intechopen.92740.

[78] M. Pratiwi, D.N. Faridah, H.N. Lioe, Structural changes to starch after acid hydrolysis, debranching, autoclaving, cooling cycles and heat moisture treatment (HMT): A review, Starch/Stärke 70 (2018) 1700028. https://doi.org/10.1002/star.201700028

[79] M.R. Brunetto, W. Orozco-Contreras, Y. Delgado-Cayama, S. Clavijo-Roa, M. Gallignani, C. Ayala-Montilla, A. Zambrano-García, Development of an analytical method for the determination of glucose, fructose and sucrose in Venezuelan samples, Revista Cubana de Química 26 (2014) 181-201.

[80] R. Sanz, G. Calleja, A. Arencibia, E.S. Sanz-Pérez, CO_2 adsorption on branched polyethyleneimine-impregnated mesoporous silica SBA-15, Appl. Surf. Sc. 256 (2010) 5323-5328. https://doi.org/10.1016/j.apsusc.2009.12.070

Credit author Statement

S.G.A: methodology, formal analysis, writing, funding acquisition
M.A.T: formal analysis and investigation
M.A: methodology, investigation and writing.
A.V.B: formal analysis, writing/review, supervision and funding acquisition

Declaration of interests

☒ The authors declare that they have no known competing financial interests or personal relationships that could have appeared to influence the work reported in this paper.

☐The authors declare the following financial interests/personal relationships which may be considered as potential competing interests:

Figures and Tables

Figure 1. SEM images of (A) potato and (B) corn starch granule.

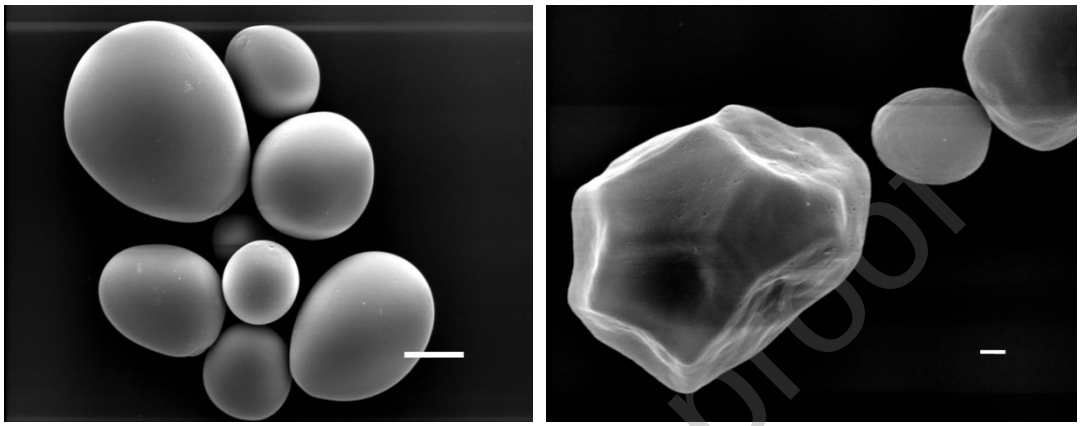

Figure 2. (A) XRD patterns and (B) FTIR spectra of (a) potato and (b) corn starches.

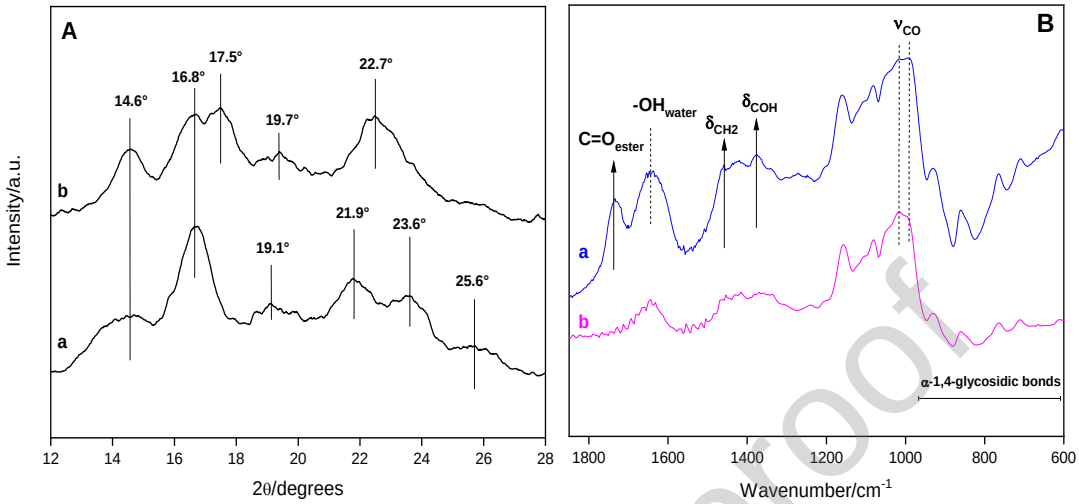

Figure 3. Curves of sample (A) mass loss and (B) derived from the mass with respect to temperature, plotted against heating temperature for (a) potato and (b) corn starches.

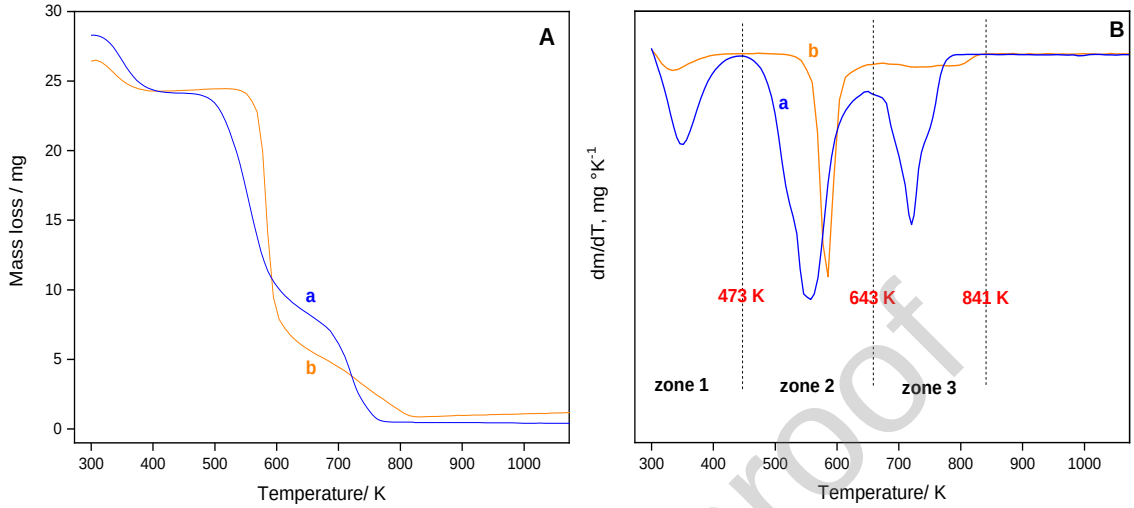

Figure 4. Microscopic images of corn starch solution at different pH and temperatures: neutral (A, B and C); basic (D, E and F) and acid (G, H and I) medium.

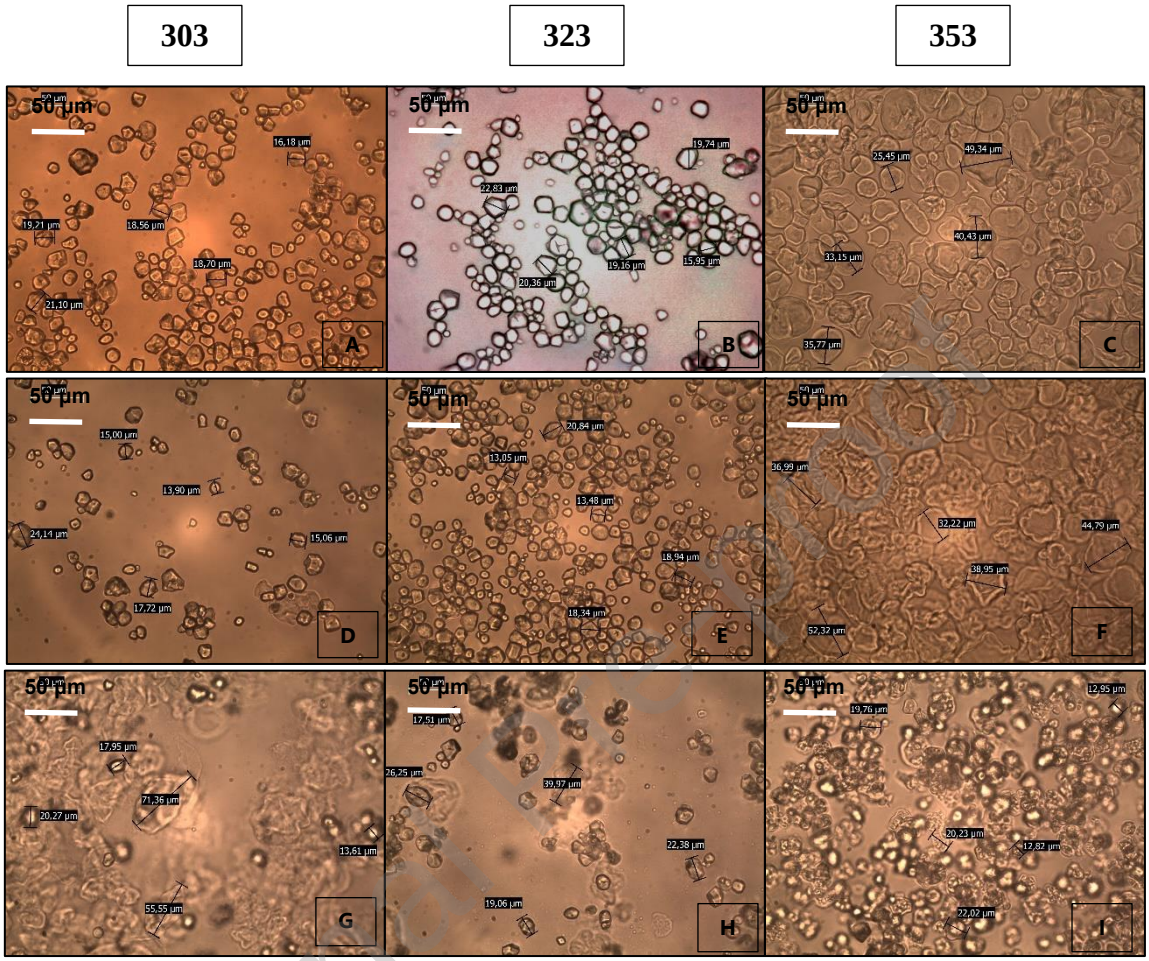

Figure 5. Microscopic images of potato starch solution at different pH and temperatures: neutral (A, B and C); basic (D, E and F) and acid (G, H and I) medium.

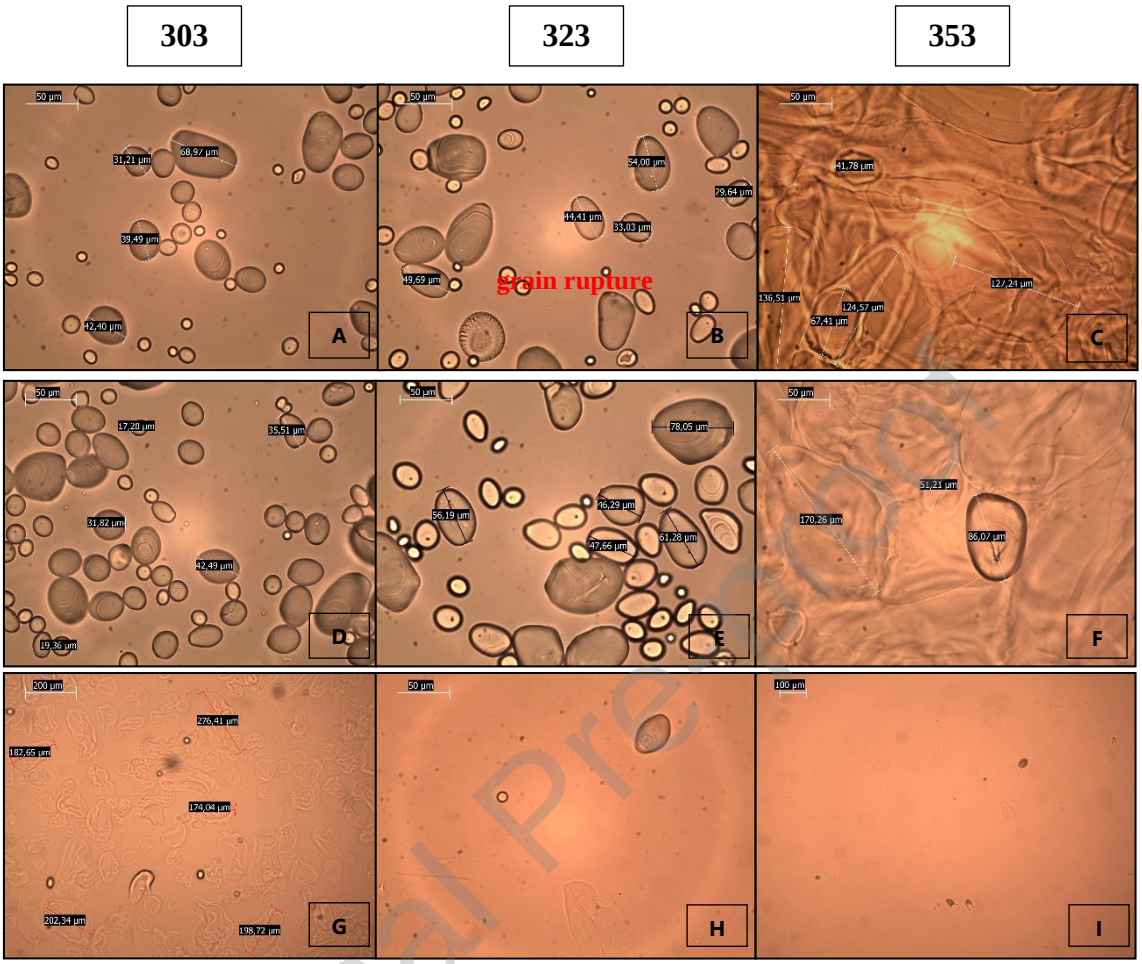

Figure 6. Microscopic images of potato starch modified with ethanol at different temperatures and in neutral (A, D and C), basic (D, E and F) and acid (G, H and I) medium.

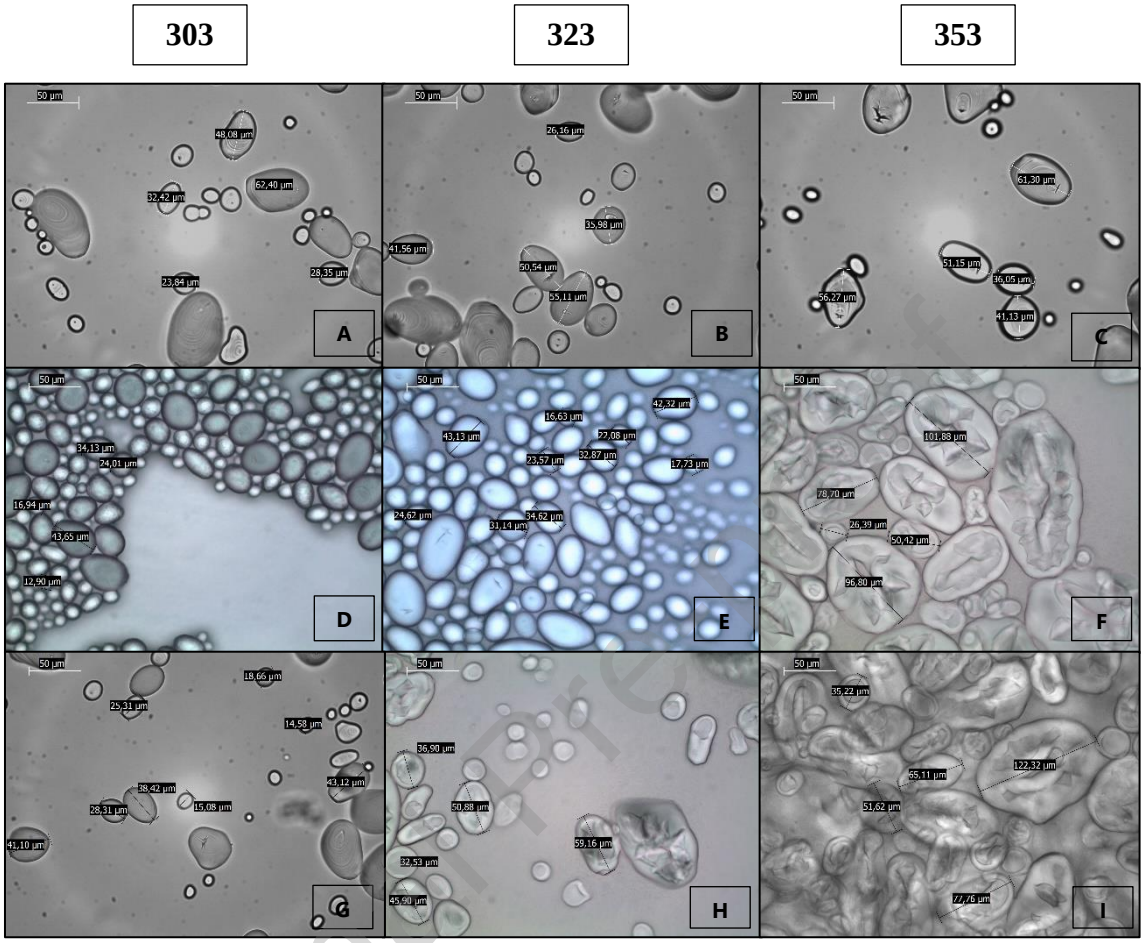

Figure 7. Microscopic images of corn starch solution at different pH and temperatures with ethanol addition: neutral (A, B and C); basic (D, E and F) and acid (G, H and I) pH.

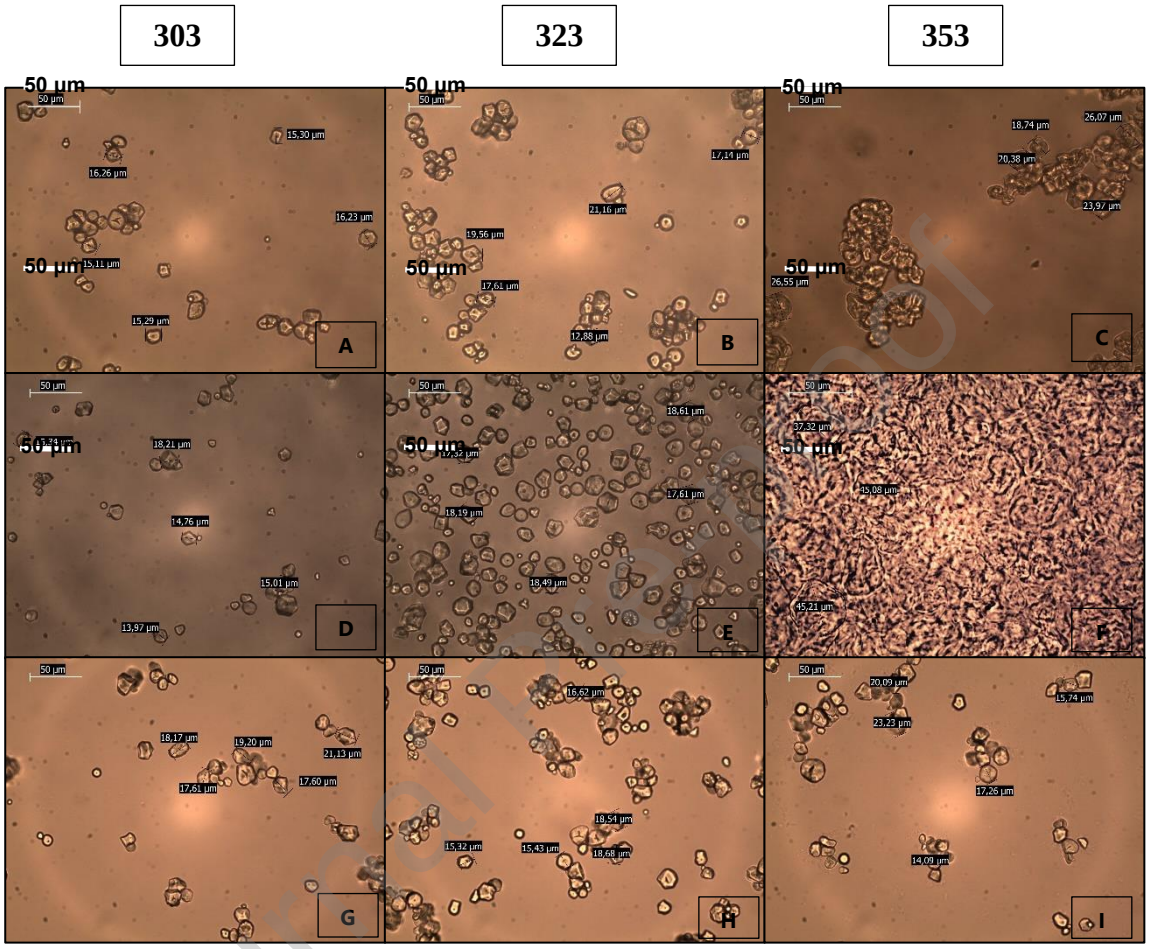

Figure 8. N_2 isotherms at 77 K for samples synthesized with potato starch in (A) neutral or (B) acidic synthesis medium of (a) P18, (b) P18/14/Et, (c) P18/14, (d) P18/14/HCl, (e) P4/14/HCl and (f) P18/2/HCl samples.

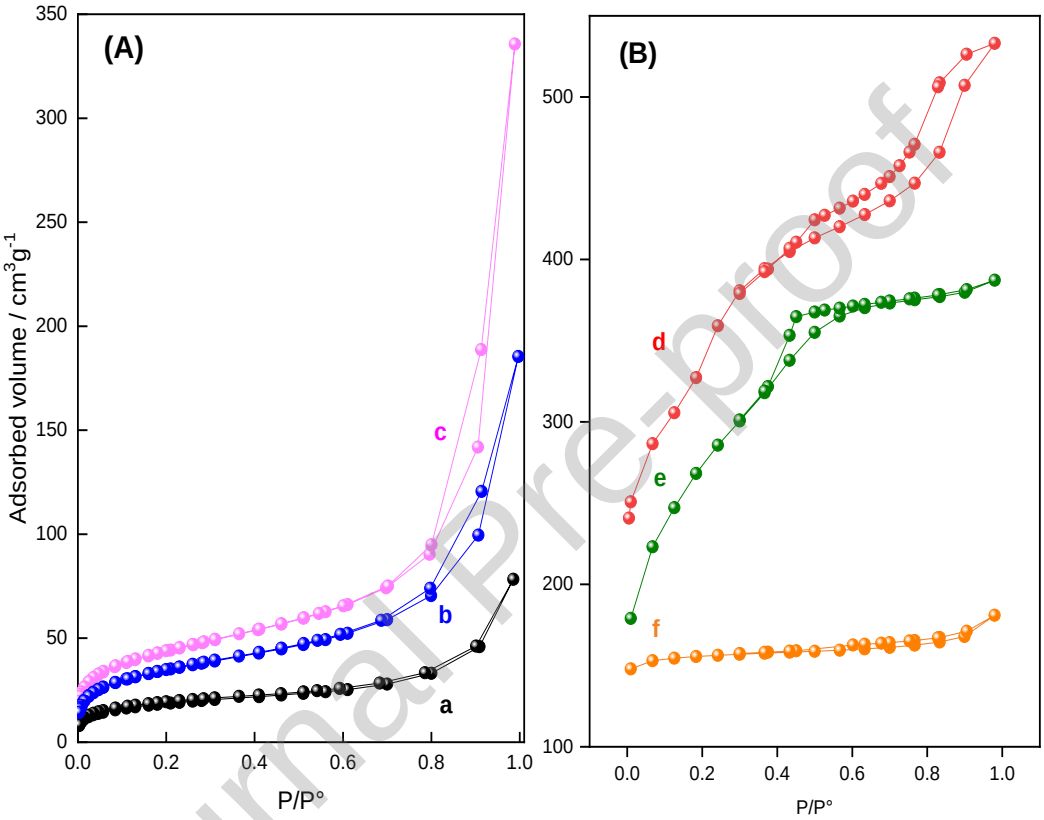

Figure 9. TEM images of P18/14 sample. Conditions of synthesis: 18 h at 353 K of gelation and 14 h at 298 K of retrogradation with potato starch.

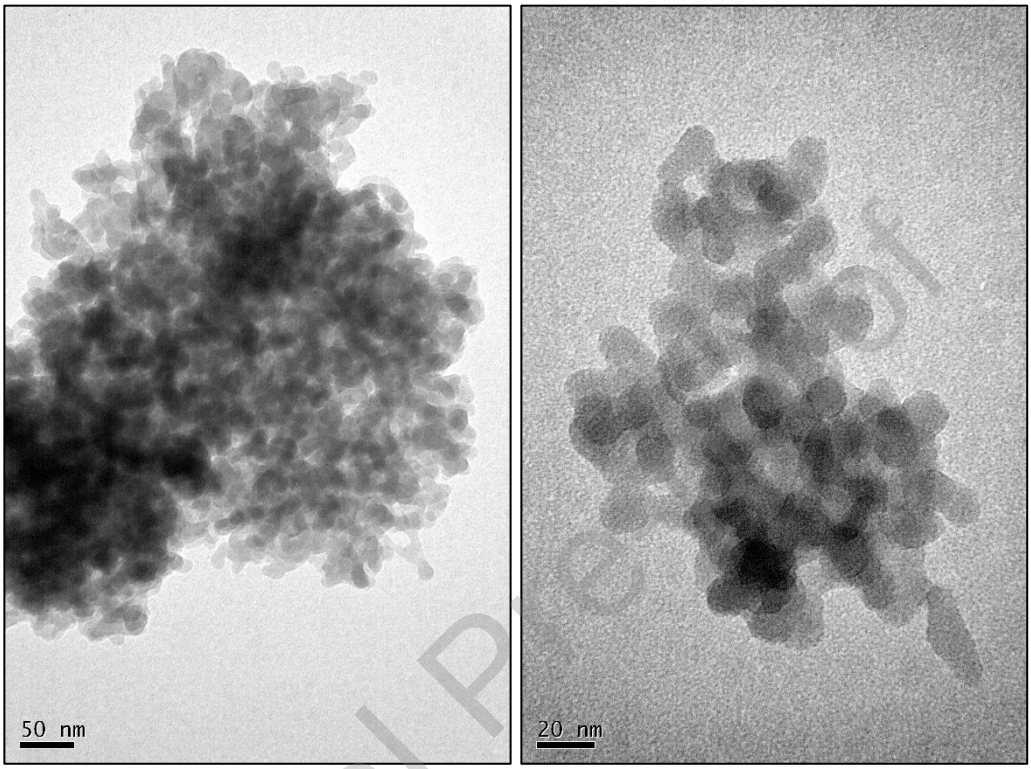

Figure 10. TEM images of P4/14/HCl sample. Conditions of synthesis: 4 h at 353 K of gelation and 14 h at 298 K of retrogradation with potato starch and HCl 37 wt. %.

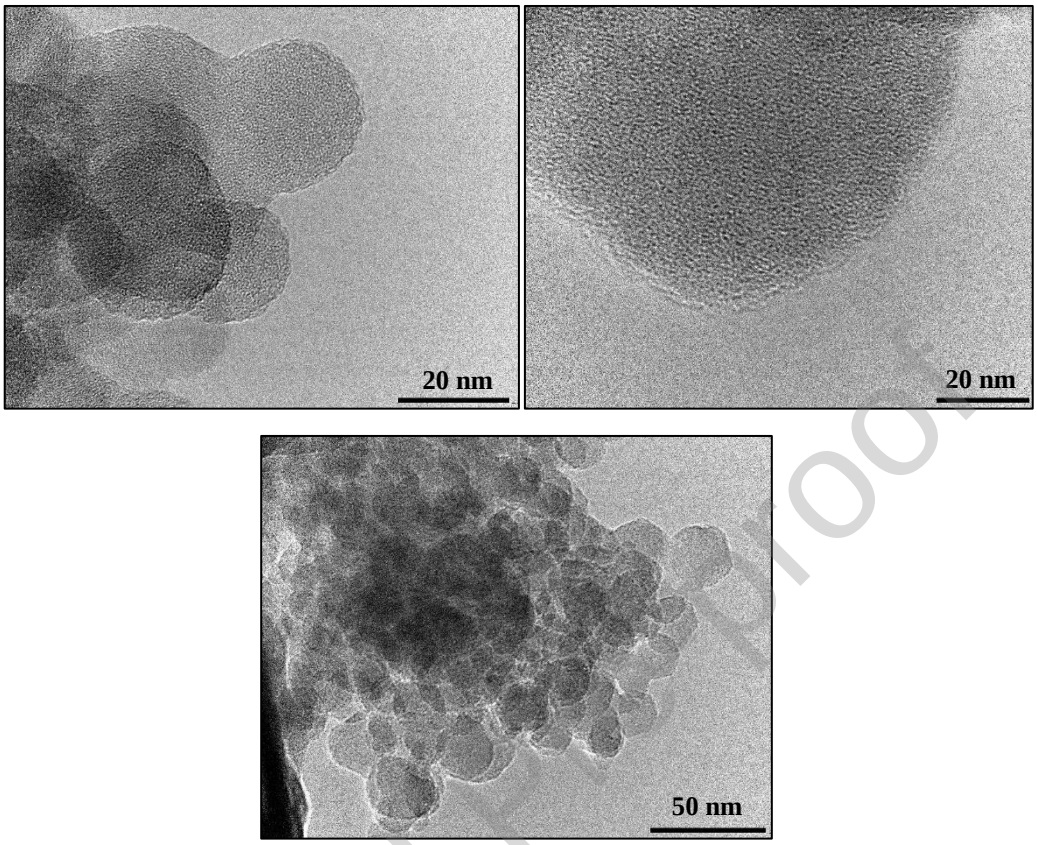

Figure 11. N_2 isotherms at 77 K for samples synthesized with corn starch in (A) neutral and (B) acidic synthesis medium of (a) C18/14, (b) C18, (c) C18/14/Et, (d) C18/2/HCl, (e) C18/14/HCl and (f) C18/14/HCl samples.

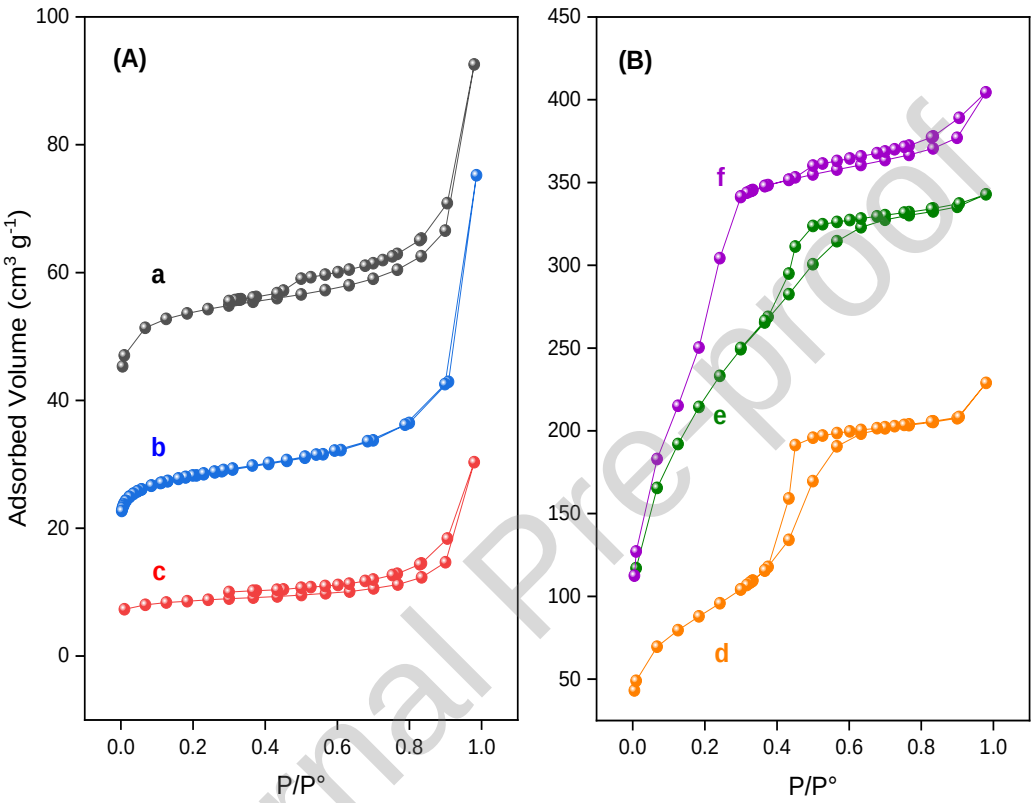

Figure 12. TEM images of C4/14/HCl sample. Conditions of synthesis: 4 h at 353 K of gelation and 14 h at 298 K of retrogradation with corn starch and HCl 37 wt. %.

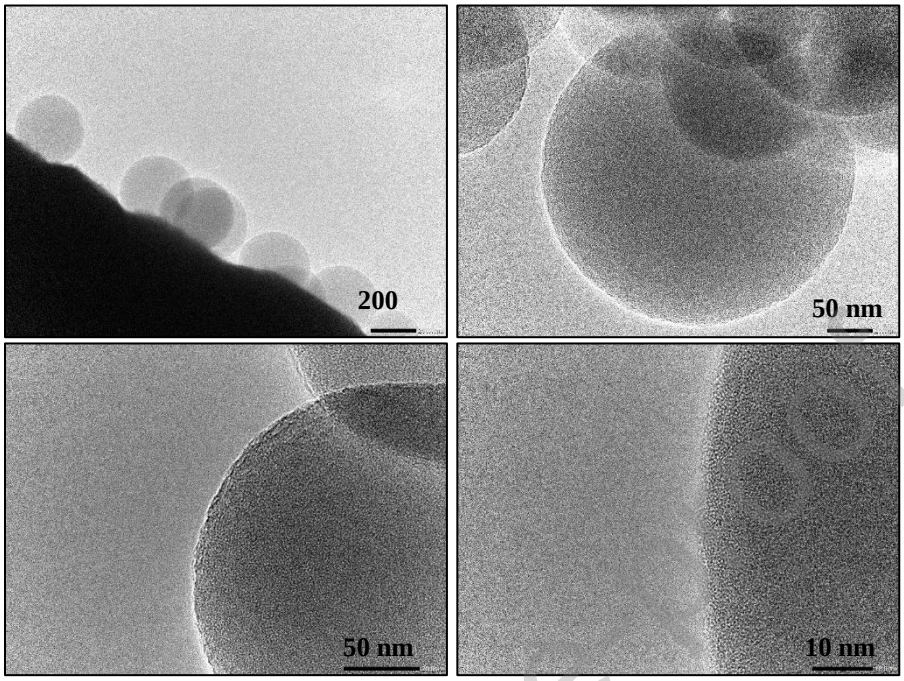

Figure 13. Scheme of the possible reactions that occur during the synthesis in acid medium.

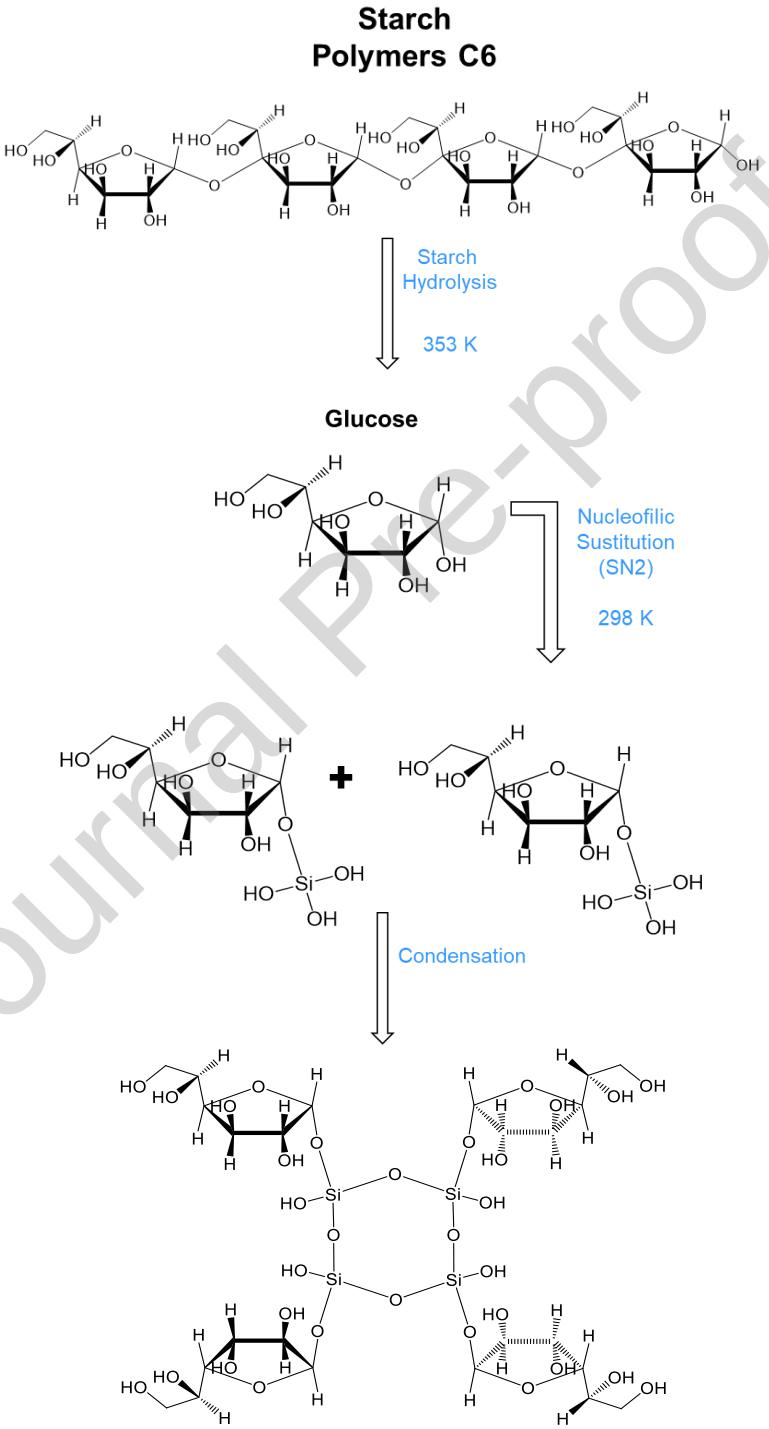

Figure 14. Breakthrough curves corresponding to CO_2 adsorption on (a) MCM41-CTAB, (b) C4/14/HCl, (c) C18/14/HCl, (d) P18/14/HCl, (e) P4/14/HCl, (f) P18/2/HCl and (g) C18/2/HCl adsorbents. Conditions: 100 mg of adsorbent, 25 cm^3 min^{-1}, 373 K and 30 % CO_2/He.

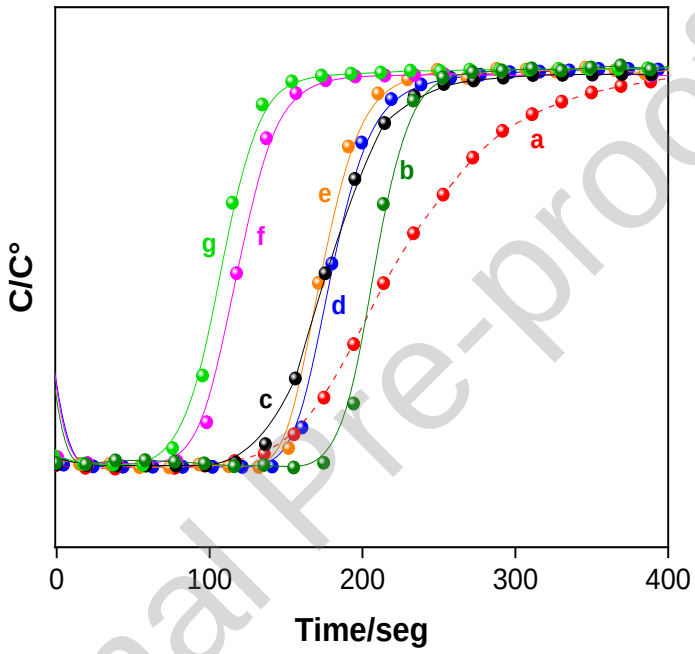

Table 1. Nomenclature of silica samples and synthesis conditions used.

Starch	Sample Name	Gelatinization[(a)] t_g (h)	Retrogradation[(b)] t_r (h)	Aggregates
Potato (P)	P2	2	-	-
	P4	4	-	-
	P18	18	-	-
	P18/2	18	2	-
	P18/14	18	14	-
	P18/14/Et	18	14	EtOH
	P18/2/HCl	18	2	HCl
	P18/14/HCl	18	14	HCl
	P4/14/HCl	4	14	HCl
Corn (C)	C2	2	-	-
	C4	4	-	-
	C18	18	-	-
	C18/25	18	2	-
	C18/14	18	14	-
	C18/14/Et	18	14	EtOH
	C18/2/HCl	18	2	HCl
	C18/14/HCl	18	14	HCl
	C4/14/HCl	4	14	HCl

[(a)] The temperature of gelatinization was 353 K, and [(b)] the retrogradation temperature was 298 K.

Table 2. Textural properties of samples prepared with potato starch.

Samples	S_{BET}[(a)]/m^2g^{-1}	V_P[(b)]/cm^3g^{-1}	D_P[(c)]/nm
P18	34.2	0.09	23.8
P18/14	130.0	0.49	22.5
P18/14/Et	17.1	0.04	15.1
P18/14/HCl	639.3	0.28	6.3
P4/14/HCl	708.6	0.38	3.9
P18/2/HCl	350.8	0.05	6.8

(a) Surface specific area, calculated by BET method, (b) Pore volume, determined by BJH method and (c) Pore diameter.

Table 3. Textural properties of samples prepared with corn starch.

Samples	S_{BET}[(a)]/m^2g^{-1}	V_P[(b)]/cm^3g^{-1}	D_P[(c)]/nm
C18	26.9	0.08	13.7
C18/14	310.1	0.07	7.1
C18/14/Et	25.8	0.04	7.9
C18/14/HCl	752.0	0.29	3.7
C4/14/HCl	1018.1	0.15	5.6
C18/2/HCl	322.1	0.39	4.0

(a) Surface specific area, calculated by BET method, (b) Pore volume, determined by BJH method and (c) Pore diameter.

Table 4. Dioxide carbon adsorption results.

Samples	Q_{ads} [a] (mg CO_2 g^{-1}_{ads})	Q_{ads}/S_{BET} (mg CO_2 m^{-2})
MCM41-CTAB	168.6	0.13
P4/14/HCl	135.7	0.19
P18/14/HCl	139.1	0.22
P18/2/HCl	40.3	0.11
C4/14/HCl	150.2	0.15
C18/14/HCl	131.4	0.17
C18/2/HCl	37.0	0.11

(a) The adsorbed CO_2 amount per gram of adsorbent.

GRAPHICAL ABSTRACT

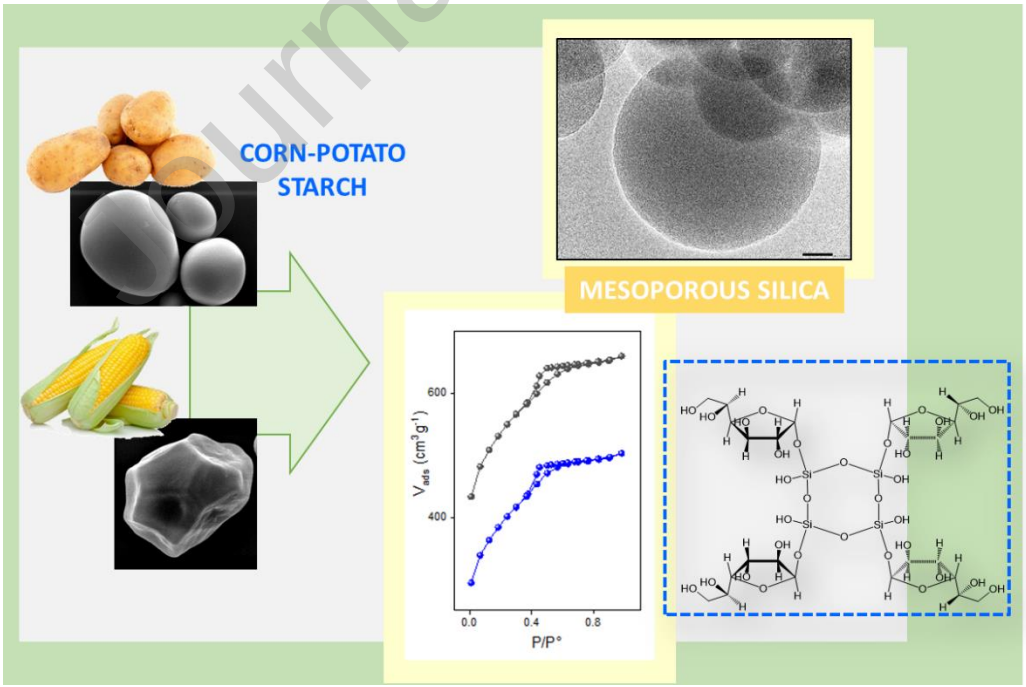

Highlights

1. With potato starch, mesoporous SiO_2 was obtained with a surface area of 708.6 m^2g^{-1}
2. With corn starch, mesoporous SiO_2 was obtained with a surface area of 1018.1 m^2g^{-1}
3. The amount of CO_2 adsorbed at 373 K was comparable with MCM41-CTAB
4. The synthesis must be carried out in an acid medium and retrograding the starch.